Science of the Total Environment 938 (2024) 173493

Contents lists available at ScienceDirect

Science of the Total Environment

journal homepage: www.elsevier.com/locate/scitotenv

Contamination of depressional wetlands in the Mpumalanga Lake District of South Africa near a global emission hotspot

C.J. Curtis [a,*], N.L. Rose [a,b], H. Yang [b], S. Turner [b], K. Langerman [a], J. Fitchett [c], A. Milner [d], A. Kabba [b], J. Shilland [b]

[a] Department of Geography, Environmental Management and Energy Studies, University of Johannesburg, Auckland Park, 2006 Johannesburg, South Africa
[b] Environmental Change Research Centre, Department of Geography, University College London, Gower Street, London WC1E 6BT, UK
[c] School of Geography, Archaeology and Environmental Studies, University of the Witwatersrand, 1 Jan Smuts Avenue, Braamfontein 2050, South Africa
[d] Department of Geography, Royal Holloway University of London, Egham, Surrey TW20 0EX, UK

HIGHLIGHTS

- South African Ramsar wetlands occur in global power station emissions hotspot.
- Sediments investigated for contamination by trace metals & sulphur over >100 years.
- Mercury and sulphur in sediments closely track emission increases since 1970s.
- Low contaminants in local coals and climatic recirculation minimise deposition.
- Hydroperiod and surface hydrology determine pollutant input and preservation.

GRAPHICAL ABSTRACT

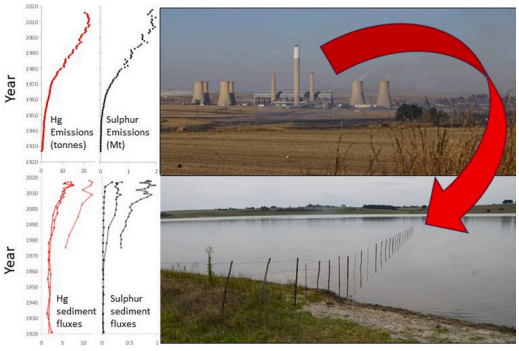

ARTICLE INFO

Editor: Abasiofiok Mark Ibekwe

Keywords:
Atmospheric deposition
Chromium
Mercury
SCPs
^{15}N
Sulphur

ABSTRACT

The Mpumalanga Lake District (MLD) of South Africa hosts a regionally unique cluster of water bodies of great importance for wetland biodiversity. It is also located close to a global hotspot for coal-fired power station emissions but the local impacts from these sources of pollution are poorly understood. Sediment cores from three contrasting wetlands were ^{210}Pb dated and analysed for a range of contaminants linked to fossil fuel combustion, including trace elements, Hg, sulphur and spheroidal carbonaceous fly-ash particles (SCPs). At the two sites with pre-industrial (1900) baseline sediments, Pb, Zn and especially Cr concentrations and fluxes showed significant increases in the impact period (post-1975). Mercury showed the greatest proportional increase in flux (>4-fold) of all trace metals. Mercury and sulphur concentrations and fluxes showed highly significant correlations with emissions over the corresponding periods, while SCPs in sediments also closely tracked emissions. In a global context, levels of sediment contamination are relatively minor compared with other heavily industrialised regions, with only Cr exceeding the sediment Probable Effects Concentration for biological impact post-1975. Despite the relatively large increases in Hg, concentrations do not reach the Threshold Effects Concentration. The unexpectedly low levels of contamination may be due to i) low levels of many trace contaminants in South African coals compared to global averages, ii) prevailing recirculation patterns which transport pollution away

* Corresponding author.
E-mail address: cjcurtis@uj.ac.za (C.J. Curtis).

https://doi.org/10.1016/j.scitotenv.2024.173493
Received 13 March 2024; Received in revised form 20 May 2024; Accepted 22 May 2024
Available online 23 May 2024

from the study area during the wet season, minimising wet deposition, and iii) pollutant remobilisation through desiccation of wetlands or volatilization. The effects of hydrology and sediment accumulation rates lead to differential transport and preservation of organic-associated and more volatile contaminants (e.g. Hg, S) relative to non-volatile trace elements in wetlands of the MLD. The greatest fluxes of Hg and S are recorded in the site with the highest catchment: lake area ratio, lowest salinity and greatest sediment organic matter content.

1. Introduction

Few studies on the environmental impacts of power generation from fossil fuels have been undertaken in the southern hemisphere. South Africa has the largest industrialised economy in Africa and one of the largest in the southern hemisphere - with major industries including the mining of coal, gold, platinum and other precious metals, energy generation, petrochemical industries (coal liquefaction) and pyrometallurgical smelters (Venter et al., 2017; Kok et al., 2021). The bulk of South Africa's energy is generated by a fleet of coal-fired power stations, located mainly in the Highveld region of Mpumalanga to the east of Johannesburg (Fig. 1): 83 % of coal production and 12 of the country's 15 coal-fired power stations are found here. Unlike many countries, South Africa also has very large, new coal-fired power stations under construction in the Highveld coalfields (Kusile, 4800 MW) and in the Lephalale area of Limpopo province, to the north of Gauteng (Medupi, 4788 MW). The national power utility Eskom has been claimed to be the world's most polluting company in terms of SO_2 emissions, at c. 1.6 Mt exceeding the combined emissions of the USA and China in 2019–2020 (Myllyvirta, 2021), with around 80 % emitted from Highveld power stations (Simelane and Langerman, 2024). One of the two SASOL coal liquefaction plants (Secunda), claimed to be the world's largest point source emitter of greenhouse gases and other pollutants (with greater emissions than over 100 individual low emission countries; Sguazzin, 2020), is also found in western Mpumalanga (Fig. 1). In addition to being a global hotspot for SO_2 emissions (Fioletov et al., 2023), several studies have also identified the Highveld as a global hotspot for NO_2 emissions from fossil fuel combustion (Wenig et al., 2002; Collett et al., 2010; Lourens et al., 2012; Greenpeace, 2018). For this study, it was therefore assumed to be a major hotspot for emissions of other coal-combustion related contaminants such as trace metals, especially mercury.

The Mpumalanga province is also home to a disproportionate number of South Africa's scarce, permanent inland water bodies within the country's only “lake district”, a region of high aquatic biodiversity and endemism. Eastern Mpumalanga contains a great number of perennial pans and lakes (De Klerk et al., 2012; Foster et al., 2015) and wetlands (e.g. Verloren Valei Nature Reserve, a Ramsar site in which a new species of freshwater crab was recently described; Daniels et al., 2014). The province is a national hotspot for threatened freshwater fish species including the cichlid *Chetia brevis*, *Barbus treurensis*, and six suckermouth catfishes (*Chiloglanis* spp.; Tweddle et al., 2009). The water bodies in the region are also important for resource provision (e.g. agricultural irrigation, fishing) and eastern Mpumalanga lies within a nationally identified Strategic Water Source Area (SWSA) for surface waters (Nel et al., 2013; Le Maitre et al., 2018). However, the pollution burden from the Highveld, particularly heavy metals and organic waste, is listed as a major threat to endemic aquatic species in Mpumalanga (Tweddle et al., 2009). Some of these water bodies are known to be highly contaminated and notorious for downstream fish and crocodile deaths attributed to catchment pollution with heavy metals, pesticides and nutrients from coal mining, industry and agriculture (e.g. Loskop Dam; Dabrowski and de Klerk, 2013). More widely in South Africa the presence of trace metals has been reported for a range of aquatic biota (see Rose et al.,

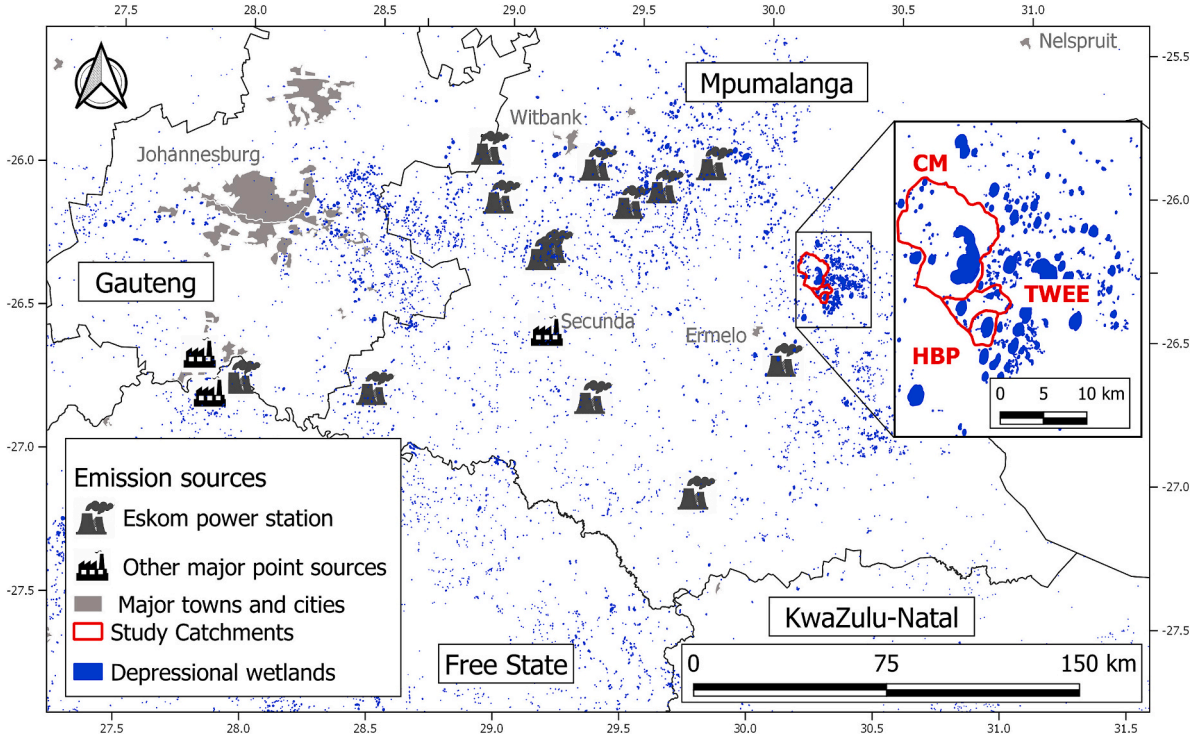

Fig. 1. Location of major atmospheric emission sources on the South African Highveld relative to sample sites in the Mpumalanga Lake District (inset). Blue shading indicates depressional wetlands classified according to the National Wetland Map 5 (Van Deventer et al., 2019). CM – Chrissiesmeer; TWEE – Tweelingspan East; HBP – Hendrik Beukes Pan. Details of the 13 Eskom power stations in Table S1.

2020 for a recent review), with "elevated" accumulation of metals in fish from the Olifants River, Mpumalanga (Kotze et al., 1999). Climate change and other threats such as population growth, water abstraction, spread of invasive species and agricultural activity exacerbate the stress on aquatic ecosystems.

Some of the strongest evidence of the links between emissions from fossil fuel combustion and impacts on water quality and aquatic ecosystems have come from long-term monitoring studies, for example in Canada, the USA and Europe (Battarbee et al., 2014; Garmo et al., 2014; Grennfelt et al., 2020). For trace metals, palaeolimnological studies have been used to link long-term changes in atmospheric deposition inputs to lakes with fossil-fuel emissions sources, for example in the UK (Yang et al., 2016) and Canada (Cooke et al., 2017). Such long-term studies are extremely scarce in the southern hemisphere, including Africa. In South Africa, water quality monitoring has been carried out at some locations since the early 1970s by the national Department of Water and Sanitation and its predecessors, but monitoring sites are sparsely distributed, many records have gaps, and only a small range of water quality parameters are widely reported (Huizenga et al., 2013; Silberbauer, 2020). Furthermore, most long-term records are for major rivers and dams, but there are only isolated "snapshot" studies looking at lakes and pans over short time periods (e.g. De Klerk et al., 2012; Foster et al., 2015; Burger et al., 2019). In addition, most published studies have looked at local contamination from catchment sources (e.g. García-Rodríguez et al., 2007) while long-range atmospheric deposition sources have been largely neglected in southern Africa – notable exceptions being the palaeolimnological studies of Kading et al. (2009) in the Western Cape, Rose et al. (2020) in Lesotho and Curtis et al. (2023) in the Eastern Cape, which show evidence of long-range transported atmospheric contaminants in the sediments of the Berg River Estuary on the west coast of South Africa, the remote lakes Letšeng-la Letsie and Mountain Lake, Matatiele, respectively, far from the major emission sources on the Highveld.

In the absence of long-term monitoring, palaeolimnological studies are often the only means to gain a longer-term perspective on contamination inputs to aquatic systems and can determine current contamination status of water bodies, identify directions and rates of change in the loadings of certain contaminants, assess the risk of contaminants to aquatic biota, and place this into its historical perspective relative to natural baselines. While high-resolution lake sediment records of trace metals and persistent organic pollutants (POPs) have been widely used in northern hemisphere studies, in South Africa such techniques have so far only been applied to a very limited number of sites (Das et al., 2008; García-Rodríguez et al., 2007; McCarthy and Venter, 2006; Rose et al., 2020; Curtis et al., 2023).

One reason for the lack of such studies may be the overall scarcity of suitable, permanent, natural inland water bodies in South Africa (Rose et al., 2021), but eastern Mpumalanga is a rare exception due to the numerous perennial lakes and pans in the Mpumalanga Lake District (MLD; Fig. 1). These pans and lakes are generally characterised by a lack of surface inflows which reduces their vulnerability to direct, catchment sources of pollution such as acid mine drainage. However, they are located in a region with numerous major point sources of atmospheric contaminant emissions, making them potentially some of the most vulnerable water bodies in the country to atmospheric pollution pathways.

To address the dual gaps in knowledge linked to historical water quality changes in perennial lakes and pans, and the role of atmospheric deposition in delivering pollutants to these hydrologically isolated systems, we investigated long-term contaminant loading in three pans in the MLD. Initially, the main focus of our study was the largest and best known lake of Chrissiesmeer, but given the lack of a priori knowledge on the suitability of the site for a palaeolimnological study (i.e. on whether a suitably intact stratigraphic record would be present), we selected two further sites in close proximity as back-up sites, to improve our chances of obtaining a good sediment record for the area. In the event that all sites provided coherent stratigraphic records, we anticipated that all would record similar signals of regional and long-range atmospheric contamination, while also providing the opportunity of comparing sites with contrasting physical and chemical characteristics. As part of a wider study including diatom analysis (Raik, 2022) to investigate biological responses to changes in atmospheric deposition of sulphur, nitrogen and trace elements, we included a wide suite of sediment analyses including geochemical (XRF) and stable isotope (^{15}N) analyses, described below.

Specifically, we aimed to:

1) assess the scale and rates of change of multiple pollutant loadings over approximately 100 years, placing current pollution into its historical perspective and providing a baseline for future studies; and
2) determine the risks these contaminants pose to aquatic organisms.

We hypothesized first (H1) that recent contaminant concentrations in the region will have increased significantly since 1950 given the subsequent major increases in emissions from fossil fuel combustion (Rose et al., 2020) and second (H2) that these will have approached or exceeded threshold or probable effects concentrations for aquatic biota, increasing the risk of adverse impacts to threatened endemic aquatic species as well as to human health via contaminated waters and fish consumption. A third hypothesis (H3) was that all three sites would record similar trends in contaminant inputs and provide spatial replication of palaeolimnological records for the MLD, given their close proximity to each other relative to the regional point sources of emissions.

To achieve these aims and test the above hypotheses, the study employed the following approaches:

- Assessment of sediment contaminant concentrations, fluxes and trends through time, with comparison of baseline (pre-construction of coal-fired power stations in the region) and impact periods (during the phase of rapid construction and increase in emissions) to determine the likely contribution of regional power station emissions (H1);
- Analysis of sediment geochemistry concentrations and trends with published threshold and probable effects concentrations (TECs and PECs) to determine the likelihood of adverse biological impacts (H2);
- Comparison of temporal trends in contaminant concentrations and fluxes with available emissions data for sulphur, nitrogen and mercury to understand pathways of pollutant delivery from atmospheric sources (H1) and interpret any between-site differences in contaminant records and preservation (H3);
- Consideration of air-mass back trajectory climatologies, geochemistry of regional coal sources (used locally in power stations) and wetland hydrology to understand the magnitude of the contamination signal in the context of similar studies globally.

2. Study area: Chrissiesmeer Lake District

Chrissiesmeer (also known as Lake Chrissie) is the centre of South Africa's only recognised "lake district" with ca. 320 lakes and pans located within a 20 km radius (Tarboton, 2009; de Klerk et al., 2016; Fig. 1). The Chrissiesmeer pans form the centre of a designated Important Bird Area (IBA) and lie within the Chrissiesmeer Protected Environment (declared on 22 January 2014, Mpumalanga Provincial Government Gazette 2251, Notice No. 19 of 2014; Birdlife, 2021). The pans support many globally and locally threatened species, with >20,000 birds roosting when the pans are wet (Tarboton, 2009; Birdlife, 2021). Thirteen species of frogs occur in the pans, with the annual "Frog Night" a major tourist attraction for the town of Chrissiesmeer (Kotzé, 2011).

In southern Africa, the term pan is generally used to describe any seasonally flooded depression which holds water after rains (Lancaster,

1978), but also includes some water bodies which may be semi-perennial and have open water for years to decades (Shaw, 1988). Uniquely in southern Africa, a large proportion of the MLD pans are perennial, with Chrissiesmeer itself being the largest. Three of only eight permanent, inland water bodies identified in South Africa in the National Biodiversity Assessment (NBA; Van Deventer et al., 2019) are in the Chrissiesmeer area (Fig. 2). The criterion used in the NBA for the designation of lakes (as opposed to pans) was a minimum depth of 2 m at "low water" with a stated average depth of 6-8 m for Chrissiesmeer, 4 m for Lake Banagher and 5 m for Tevredenpan (Grundling et al., 2008; De

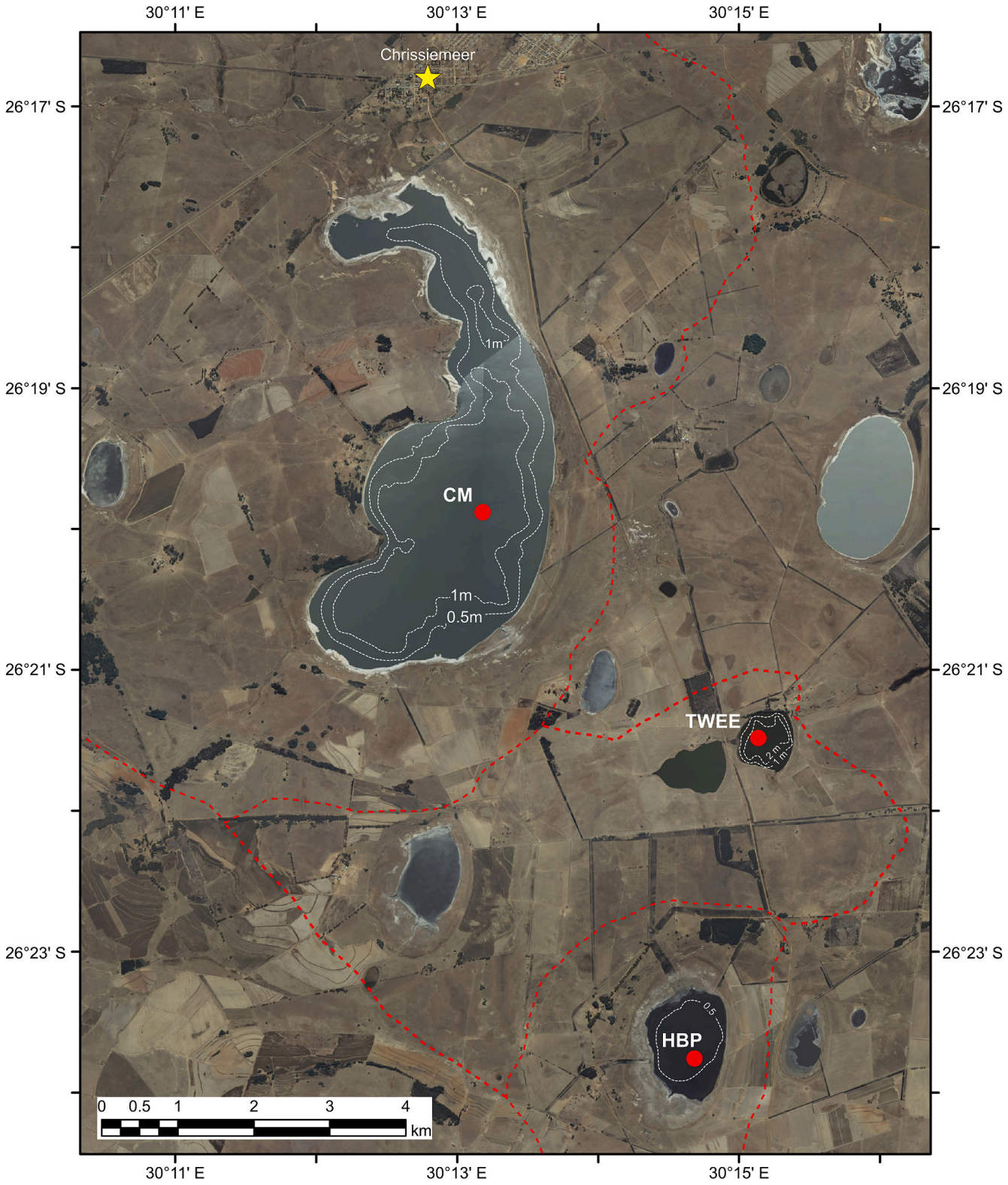

Fig. 2. Study area, bathymetric maps and coring locations for study sites (CM – Chrissiesmeer; TWEE – Tweelingspan east; HBP – Hendrik Beukes Pan). Red dotted lines indicate approximate catchment boundaries manually digitised from 1:50,000 topographic maps. Yellow star indicates the town of Chrissiesmeer.

Klerk et al., 2016). However, these are not the only (semi) perennial pans in the region; in fact De Klerk et al. (2016) cite earlier studies identifying 4628 pans in eastern Mpumalanga, of which almost half are perennial, many centred around the MLD.

The study area catchments of the MLD occur in a humid zone with mean annual precipitation in the range of 728-767 mm and mean annual A-pan evaporation of 1700-1800 mm (WR2012, 2015). The region lies in the summer rainfall zone of South Africa (Roffe et al., 2020) with wettest months in October–January when monthly precipitation can approach 100 mm, while very little rainfall falls during late autumn-winter (<10 mm per month in May–August, Meteoblue, 2024). Mean daily maximum temperatures range from 16 °C in June to 24 °C in November–January, while mean daily minimum temperatures range from 2 °C in June–July to 13 °C in December–January (Meteoblue, 2024). It is an important watershed area of South Africa with four big river systems starting in the region (Vaal, Komati, uMpuluzi and Usutu Rivers; Wellington, 1943; Kotzé, 2011) and is close to the headwaters of a nationally important strategic water source area (Nel et al., 2013). The geology underlying the study area is the Ecca Group of the Karoo Supergroup, predominantly sandstones and shales with dolerite intrusions in some areas (Foster et al., 2015), while the coal bearing Vryheid formation accounts for the presence of coal mines and power stations in the vicinity (Russell, 2008). The closest power station to the study sides is Camden (35 km from Chrissiesmeer) with another five located within 100 km and a total of 12 operational on the Highveld (Fig. 1; Table S1), the furthest one being Lethabo (229 km). In addition, a thirteenth power station with a design capacity of 4800 MW (Kusile), was still being commissioned in 2024 after the first unit came online in 2017, which will increase total regional generation capacity from 33GW to almost 38GW. Other than mining, the main land uses are primarily agricultural, with maize and cattle grazing.

The pans of the MLD are notable for their chemical and biological diversity, with saline pans in very close proximity to freshwater pans and major differences in aquatic vegetation, invertebrates, fish and birdlife often found in pans only a few hundred metres apart. Wellington (1943) highlighted the poor understanding of these spatial differences which are linked to the relative balance between precipitation, groundwater inputs or percolation losses, evaporative processes and mineral precipitation/dissolution reactions during evaporation and rewetting. An important physical control on hydrology is the catchment area to lake surface area (C:L) ratio of the pans (Russell, 2008). Chrissiesmeer has the largest C:L ratio of the pans studied by Russell (2008) which was reflected in its permanence and low salinity, compared with pans having much lower ratios which tended to be more temporary and show greater seasonal changes in salinity.

Given the lack of published data on the depth and permanence of pans in the MLD and hence their potential suitability for palaeolimnological study (i.e. the likelihood of an undisturbed sediment record), this study selected sites on the basis of bathymetric surveys undertaken by Spratt (2019; Fig. 2). Chrissiesmeer (CM) was selected as the largest pan in the area, while the back-up site of Tweelingspan East (TWEE) was selected as the deepest known site in the area (Table 1). The third site, Hendrik Beukes Pan (HBP), was selected as a second back-up site in close proximity in case the other sites did not provide suitably intact stratigraphic records. Physical and chemical details of the coring sites are presented in Table 1 and Table S2 in Supplementary information. Although major ions were not analysed in our study, Russell (2008) described both CM and HBP (DRIE-B in that study) as Na-Cl-HCO_3 dominated systems, while the paired TWEE pans are regionally unique in being more dilute and having similar proportions of Na-Ca-Mg and Cl-HCO_3-SO_4. Shorter cores obtained from TWEE indicate an abrupt textural change at c. 14-16 cm depth that was not found at the same depth in the other sites (Table 1).

3. Methods

3.1. Coring

Sediment cores were taken using an HTH gravity corer fitted with a polycarbonate tube of internal diameter 86 mm (Renberg and Hanson, 2008). The cores were extruded vertically in the field at 0.5 cm intervals. Chrissiesmeer and Hendrik Beukes Pan were cored in 2017 following bathymetric surveys of the lakes. Cores CM1 (length 26 cm) and HBPA (26.5 cm) were used for lithostratigraphic, SCP and trace metal analysis and radiometric dating while CM1 was also subsampled for $\delta^{15}N$ analysis.

Three replicated cores were taken from one location at Tweelingspan (cores = TWEE-1, 16 cm; TWEE-2, 16 cm; TWEE-3, 14 cm) in 2018 (Table 1). TWEE-1 was the master core used for radiometric dating. Core TWEE-2 was used for trace metal and SCP analysis while core TWEE-3 was retained for a separate study. Lithostratigraphic analysis of all cores was used to cross-correlate dates from TWEE-1 to the other cores.

3.2. Lithostratigraphic analyses and core chronologies

Lithostratigraphic analyses (water content; loss-on-ignition at 550 °C and 950 °C as an estimate of organic matter content and carbonate content respectively) were undertaken on each sample following standard methods (Dean Jr., 1974; Heiri et al., 2001).

Core samples were analysed for ^{210}Pb, ^{226}Ra, ^{137}Cs and ^{241}Am by direct gamma assay using ORTEC HPGe GWL series well-type coaxial low background intrinsic germanium detectors. Lead-210 was determined via its gamma emissions at 46.5 keV, and ^{226}Ra by the 295 keV and 352 keV gamma rays emitted by its daughter isotope ^{214}Pb following three weeks storage in sealed containers to allow radioactive equilibration for ^{222}Rn and ^{226}Ra. Cesium-137 and ^{241}Am were measured by their emissions at 662 keV and 59.5 keV, respectively. The absolute efficiencies of the detector were determined using calibrated sources and sediment samples of known activity. Corrections were made for self-absorption of low energy gamma rays within the sample (Appleby et al., 1992). Unsupported ^{210}Pb, from atmospheric deposition, was calculated by subtracting supported ^{210}Pb (which derives from in situ decay of ^{226}Ra) from total ^{210}Pb. Final sediment chronologies were determined from ^{210}Pb records using constant rate of supply (CRS) or constant initial concentration (CIC) models (Appleby, 2001), in combination with ^{137}Cs and ^{241}Am profiles. Derived and interpolated sediment accumulation rates (g cm^{-2} yr^{-1}) were used to convert contaminant concentrations into fluxes. For the undated core TWEE-2, LOI550 and LOI950 curves were compared with the dated core TWEE-1 and curves were found to follow very similar trends with several tie points (see Supplementary material, Fig. S1). Hence the TWEE-1 dates were used to estimate dates in core TWEE-2 by assuming similar sedimentation rates between the two cores.

Table 1
Physical characteristics and electrical conductivity (EC) of study sites and sediment core samples.

Site	Long (E)	Lat (S)	Alt (m)	Max Depth (m)	Lake area (Ha)	Cmt area (Ha)	C:L Ratio	Core length (cm)	Coring date	EC (μS/cm)
CM	30° 13′ 08.98″	26° 19′ 49.12″	1673	1.3	1283	10,591	8.3	26.0	12/08/2017	4902
HBP	30° 14′ 40.60″	26° 23′ 42.61″	1671	0.4	242	995	4.2	26.5	16/04/2018	3588
TWEE	30° 15′ 05.60″	26° 21′ 31.20″	1681	2.5	48	1953	40.0	16.0	22/11/2017	139

3.3. Sediment geochemistry and trace metal analysis

Weighed (4 d.p.) freeze-dried milled sediment (~2 g) was measured using an X-ray fluorescence spectrophotometer (Rigaku NEX CG EDXRF) for trace elements (As, Cr, Cu, Mn, Ni, Pb, Ti, V, Zn) commonly associated with South African coals (Wagner and Hlatshwayo, 2005) as well as sulphur (S). A certified or standard reference material (CRM or SRM) sediment sample of similar mass was included in each analytical run. For CM and HBP, the LKSD2 CRM was used, with mean recovery rates of ±12 % for trace metals, ±14 % for Mn and a systematic underestimate by 60–62 % for S (see later). For TWEE, the Buffalo River Sediment NIST 2704 SRM was used with a greater variation in recovery rate of ±26 % (Kabba, 2019). All analytical quality control results are presented in the Supplementary material (Table S3).

For mercury (Hg) analysis, 0.2 g of freeze-dried samples were weighed into a 50 mL polypropylene DigiTUBE (SCP Science). 8 mL aqua regia (nitric and hydrochloric acids in a molar ratio of 1:3) were added to each and gradually heated on a hotplate to 100 °C to avoid violent reaction. The sample was then digested for another 1.5 h and allowed to cool. The digested solution was diluted to 50 mL using distilled deionised water. Standard reference stream sediment (GBW07305; certified Hg value 100 ± 10 ng g^{-1}; our measured mean value 100.3 ng g^{-1}; standard deviation = 4.5 ng g^{-1}; $N = 15$) and sample blanks were digested with every 20 samples. Mercury concentrations were measured by cold vapour-atomic fluorescence spectrometry (CV-AFS) following reduction with $SnCl_2$. Standard solutions and quality control blanks were measured after every five samples to monitor measurement stability.

3.4. Spheroidal carbonaceous particles (SCPs)

SCP analysis involved sequential treatments of nitric, hydrofluoric and hydrochloric acids to remove organic, siliceous and carbonate fractions respectively, resulting in a suspension in water (Rose, 1994). A known fraction of this suspension was then evaporated onto a coverslip, mounted onto a glass slide, and the number of SCPs counted using a light microscope at 400 times magnification. Standard criteria for SCP identification were followed (Rose, 2008). SCP concentrations were calculated as the number of particles per gram dry mass of sediment (gDM^{-1}) and SCP fluxes calculated as the product of SCP concentration and bulk dry sediment accumulation rate (number of particles per cm^2 per year; cm^{-2} yr^{-1}). Analytical blanks and SCP reference material (Rose, 2008) were included with all sample digestions. The detection limit for the technique is typically <100 gDM^{-1} and calculated concentrations generally have an accuracy of c. ± 45 gDM^{-1}.

3.5. Stable isotopes of nitrogen (CM1 only)

Samples were analysed for their $\delta^{15}N$ signatures using a Flash EA 1112 and a Delta V continuous-flow gas-isotope-ratio mass spectrometer (Thermo Scientific®) in the Bloomsbury Environmental Isotope Facility, UCL. Samples of 10–20 mg were accurately weighed into tin capsules which were dropped into a furnace held at 1020 °C and burned with a pulse of oxygen at about 1800 °C. The released gases were carried in a stream of helium through an oxidant (granular chromium oxide combustion reagent) to complete combustion; silvered cobalt chemical traps to remove sulphur and halogens; a copper reduction furnace to trap excess oxygen and to convert the formed NO_x to N_2 for analysis; and a magnesium perchlorate drying tube which also contained some Carbosorb to remove CO_2. Finally, the gases passed through a gas chromatograph (GC) column before passing through a Thermal Conductivity Detector (TCD, to obtain TN%) to then enter the mass spectrometer via a CONFLO IV interface. The results were calibrated against laboratory and international standards (i.e. IAEA-600, IAEA-N1, IAEA-N2, USGS40, OEA alanine). Nitrogen isotope ratios are reported in the conventional delta-notation, in per mil (‰) with respect to atmospheric N_2 (Air).

3.6. Transport climatologies and air mass back trajectories

Transport climatologies representative of dry and wet deposition conditions were developed using back trajectories calculated by NOAA's HYSPLIT trajectory model (Draxler and Hess, 1998; Stein et al., 2015). Trajectories were run at 5-year intervals from 1950 to 2015 (the last complete five year period before the date of coring). NCEP's reanalysis meteorological data at 2.5° resolution was used. Trajectories for the dry deposition transport climatology were started 10 m above ground level in order to represent conditions at the surface where the dry deposition of aerosols and gases occurs, but sufficiently high above the surface so that most of the trajectories did not hit the ground. The back trajectories were run for 48 h, at 12-h intervals (02:00 and 14:00 local time) throughout the selected years. Trajectories for the wet deposition conditions were started 1000 m above ground level and run backward for 36 h, starting at 14:00 local time, at 24-h intervals. Trajectories were only run for October–April, the wet season in that region according to Roffe et al. (2020), starting at 14:00 each day when convective rainfall is often initiated (Rouault et al., 2012). The starting point of 1000 m above the ground was selected because the average height of the convective boundary layer on the Highveld (as measured at Elandsfontein, 80 km west of Chrissiesmeer and at a similar altitude) ranges between 900 m in the morning (9:00) and 1700 m in the late afternoon (15:00–17:00) (Korhonen et al., 2013).

Frequency plots and wind sector allocations were created using Openair in R (Carslaw, 2015; Carslaw and Ropkins, 2012). The frequency plots show the proportion of trajectories arriving at Chrissiesmeer that travel over 0.5° by 0.5° grid squares. Trajectories are allocated to the wind sector in which they spend the most time, provided they spend at least 15 of the 36/48 h in that sector. A trajectory that spends <15 h in any one sector is considered to be 'unallocated'.

3.7. Statistical analysis and temporal comparison

For statistical comparison of temporal change in contaminant concentrations and fluxes, the sediment record was divided into two key periods; i) a baseline period prior to 1900 before any coal-fired power stations were constructed within South Africa (hereafter "baseline") and ii) a common period of rapidly increasing emissions from coal-fired power stations, from 1975 (coincident with the basal date of the sediment record in TWEE - see below), to the present (2017–2018 when core samples were obtained), hereafter "impact period". Differences in mean concentrations or fluxes between the two time periods were assessed using Levene's test for homogeneity of variance and the independent samples *t*-test in SPSS, with significant differences assumed for $p < 0.05$. Comparisons of LOI550 (organic matter) between sites used the independent samples Kruskal-Wallis test for non-normally distributed data. Correlations between contaminant concentrations or fluxes in sediments and power station emissions for the corresponding years were calculated using Pearson's correlation coefficient (r, two-tailed) in SPSS.

4. Results

4.1. Chronology

Radiometric dating indicates core chronologies extending back to 1853 ± 37 (164 years) for Chrissiesmeer, 1975 ± 12 (43 years) for Tweelingspan and 1873 ± 33 (144 years) for Hendrik Beukes Pan (see Fig. S2 and Tables S4-S6 in Supplementary material for full details). For core CM1, sedimentation rates calculated by the radiometric data suggest that from the 1880s to the 1990s, sedimentation processes were relatively stable with a mean rate of 0.051 g cm^{-2} yr^{-1} which is followed by a steep increase to 0.123 g cm^{-2} yr^{-1} over the last 20 years. At Hendrik Beukes Pan (core HBPA), the CRS model suggested that sedimentation rates of the core show a general increasing trend from 0.02 g cm^{-2} yr^{-1} in the 1870s to 0.14 g cm^{-2} yr^{-1} at the time of coring, with a

small peak in the 1910s reaching 0.148 g cm^{-2} yr^{-1} and a relatively stable period with a mean rate at 0.076 g cm^{-2} yr^{-1} from the 1930s to the 1970s. At Tweelingspan, the short sediment record showed relatively uniform sedimentation rates with a mean at 0.087 g cm^{-2} yr^{-1} over c.40 years, with minor fluctuations in the last 15 years. According to the CRS model, at the coring locations the unsupported ^{210}Pb fluxes to the sediments are TWEE: 248.2 ± 33.5, CM: 269.5 ± 8.7 and HBP: 233.9 ± 9.7 Bq m^{-2} yr^{-1}, respectively, suggesting no major between-site differences due to the effects of sediment focusing.

4.2. Trace elements

4.2.1. Concentrations, trends and fluxes

For the 12 trace and major elements selected for this study, the range of concentrations (minimum, maximum), mean baseline values (pre-1900) and mean concentrations for the impact period (1975–2017/18) are presented in Table 2. With the exception of V (all sites), Cu at HBP and Mn at CM, all elements at all sites showed peak concentrations between 1978 and the surface of the cores (2017–18). Potentially anomalous peaks in Pb and possibly Zn concentrations in near surface sediments at Chrissiesmeer (Fig. 3) were checked by XRF re-analysis and found to be correct, but for Pb the large outlier (>10× higher than other samples) was excluded from further statistical analysis of temporal change.

At the two sites with baseline samples (CM and HBP), all elements except for V showed a significant difference in concentrations (*t*-test, $p = 0.05$) between the two time periods for at least one site, but only four elements showed significantly higher concentrations in the impact period in both sites; Cr, Hg, Pb and Zn (Table 2, Fig. 3). HBP also had significantly higher impact period concentrations for As, Mn, Ni and Ti and a significantly lower concentration of Cu (Table 2). For S, a significant increase was found only in CM. Mercury and sulphur are considered separately below where they are compared with power station emissions data.

Relative to mean baseline concentrations, the largest average proportional increases during the impact period were seen for Cr (28 and 33 % at CM and HBP; Table 2, Fig. 3) and As (30 %) but As was statistically significant ($p = 0.05$) only for HBP. At CM, the proportional increase in Pb and Zn was identical to Cr at 28 %, but at HBP there were smaller increases in Zn (13 %) and Pb (12 %). All other changes in mean concentrations between baseline and impact periods were smaller than 10 %. The greatest peak concentrations relative to baseline means were

Table 2
Summary of trace element (TE) concentrations and fluxes with *t*-test comparison of means for baseline (pre-1900) and impact (post-1975) periods. SE = standard error. Yellow shading indicates exceedance of TEC, red indicates exceedance of PEC (see Supplementary material Table S7 for published TEC and PEC values). Bold figures (%) indicate statistically significant changes at $p < 0.05$ ($p < 0.01$ for fluxes at HBP). LOI550 = loss on ignition at 550 °C, representing organic matter (%) while SAR = sediment accumulation rate (g cm^{-2} yr^{-1}).

		CONCENTRATIONS (µg g^{-1}, except for Hg ng g^{-1})										FLUXES (µg or ng (Hg) cm^{-2} yr^{-1})				
		Whole Core		Peak	Baseline		Impact		t-test		%Inc	Baseline		Impact		
TE	Site	Min	Max	year	Mean	SE	Mean	SE	p	Δ%	Peak	Mean	SE	Mean	SE	Δ%
	CM	3.3	7.4	2013	4.4	0.23	5.3	0.28	0.072	22	69	0.18	0.06	0.40	0.03	**120**
As	HBP	3.2	6.2	2017	4.0	0.12	5.3	0.13	0.000	**30**	52	0.14	0.04	0.57	0.04	**303**
	TWEE	3.7	5.4	2009			4.5	0.09						0.42	0.01	
	CM	107	177	2008	115	2.8	147	4.2	0.001	**28**	54	4.68	1.60	11.5	0.87	**146**
Cr	HBP	80	140	2014	96	1.7	127	2.5	0.000	**33**	46	3.47	0.91	13.7	1.09	**294**
	TWEE	119	160	1989			138	2.0						12.9	0.31	
	CM	40.1	60.0	2013	50.1	1.2	53.2	1.5	0.289	6	20	1.96	0.65	4.14	0.30	**111**
Cu	HBP	28.0	36.3	(1823)	33.5	0.3	31.4	0.7	0.017	**-6**	8	1.22	0.31	3.39	0.30	**178**
	TWEE	31.5	39.4	2010			36.1	0.4						3.37	0.06	
	CM	15.3	76.9	2015	28.1	7.6	62.8	2.6	0.001	**123**	174	1.09	0.46	4.97	0.40	**355**
Hg	HBP	20.7	52	2016	28.0	0.9	38.7	2.3	0.045	**38**	86	2.08	1.1	4.40	0.52	**112**
	TWEE	69.1	119.3	2018			104	5.2						9.76	0.79	
	CM	712	1000	1967	926	19.4	875	18.0	0.150	-6	8	37.48	12.82	67.8	4.68	**81**
Mn	HBP	663	737	2011	693	4.1	712	4.2	0.005	**3**	6	24.56	6.30	75.8	5.05	**209**
	TWEE	67	559	2018			215	32.7						21.0	3.39	
	CM	37.7	50.3	2000	44.1	0.7	45.4	0.8	0.403	3	14	1.76	0.60	3.53	0.25	**100**
Ni	HBP	39.0	44.9	2011	41.5	0.2	43.4	0.4	0.000	**5**	8	1.47	0.35	4.62	0.31	**215**
	TWEE	31.9	40.6	1989/95			37.3	0.4						3.48	0.05	
	CM	19.4	395	2017	20.7	0.5	26.6	0.5	0.000	**28**	1806	0.85	0.29	2.01	0.15	**137**
Pb	HBP	23.6	28.6	2014	24.7	0.1	27.7	0.2	0.000	**12**	16	0.90	0.23	2.95	0.20	**227**
	TWEE	23.0	27.4	1989			25.1	0.2						2.35	0.04	
	CM	3470	5810	1978	4654	81.3	4249	143.3	0.142	-9	25	190.1	63.5	328.5	23.0	**73**
Ti	HBP	5330	6220	2011	5575	39.8	5821	76.7	0.004	**4**	12	197.5	50.1	620.6	41.9	**214**
	TWEE	3740	4620	1978			4223	39.6						394.4	6.10	
	CM	96	160	1946	115	3.5	112	2.2	0.428	-3	39	4.66	1.52	8.74	0.66	**88**
V	HBP	79	122	1933	100	2.3	104	3.8	0.392	4	22	3.85	0.93	10.9	0.65	**184**
	TWEE	60	107	1975			75	1.8						7.05	0.22	
	CM	68	131	2017	74	1.7	94	2.8	0.001	**28**	78	3.00	1.03	7.47	0.74	**149**
Zn	HBP	88.9	105	2017	90	0.2	102	0.7	0.000	**13**	16	3.24	0.82	10.9	0.79	**238**
	TWEE	75	87	2003			80	0.6						7.53	0.15	
	CM	183	5470	1996	214	13.0	3373	260.2	0.000	**1473**	2451	9.40	3.21	253.3	17.3	**2595**
S	HBP	203	1250	2017	313	14.4	389	87.4	0.290	24	299	8.83	2.42	45.4	13.9	414
	TWEE	4140	8930	2015			6911	265.4						661.2	35.4	
LOI	CM	7.97	14.09	2012	8.47	0.20	12.09	0.20	0.009	**43**	66					
550	HBP	9.33	12.27	2015	9.49	0.08	10.04	0.26	0.641	6	29					
	TWEE	19.91	30.14	2018			24.79	0.61								
	CM	0.01	0.123	2017	0.040	0.013	0.075	0.011	0.153	**89**	212					
SAR	HBP	0.02	0.148	1913	0.036	0.016	0.106	0.014	0.016	197	313					
	TWEE	0.07	0.109	2009			0.094	0.004								

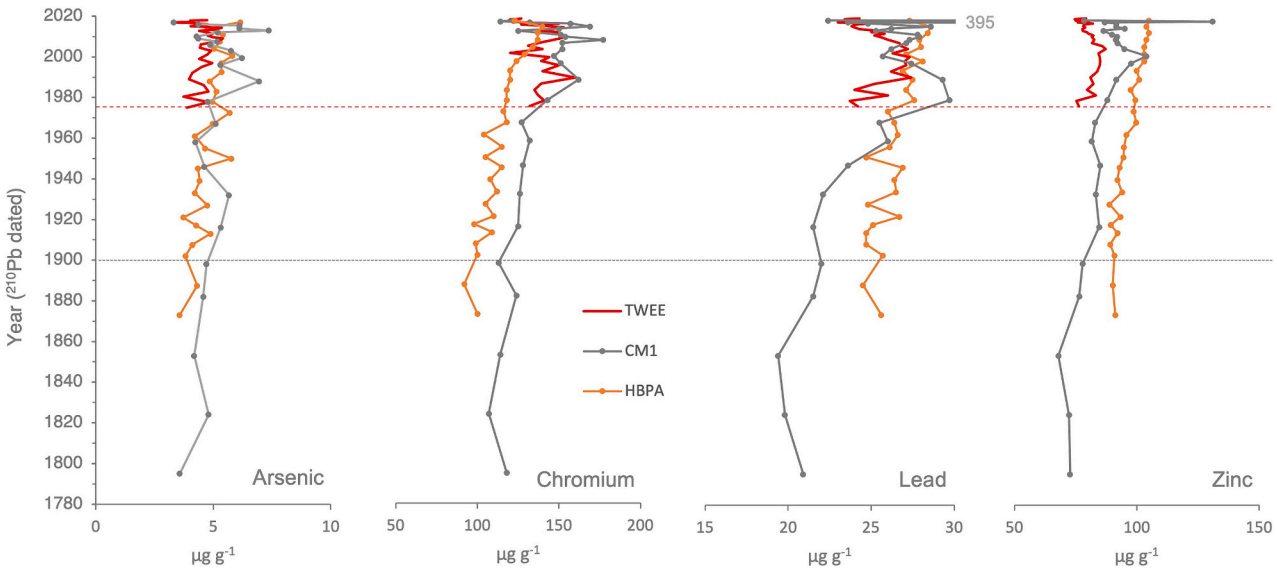

Fig. 3. Selected trace element concentrations in sediment cores CM (grey), HBP (orange) and TWEE (red). Samples below lower dotted line (1900) used to calculate baseline concentrations for CM and HBP. Samples above upper dotted line (1975) used to represent impact period in all three sites. Dates below 1853 (CM) and 1873 (HBP) approximated using basal SAR. For Pb, an anomalous peak concentration of 395 µg g^{-1} is omitted from the plot for clarity (see text for discussion). Plots of Hg are compared separately with emissions trends in Fig. 4 below.

found for As (69 and 52 % higher), Cr (54 and 46 %), Pb (43 and 16 %) and Zn (78 and 16 %) for CM and HBP respectively. In CM, most elements showed a sharp decline in concentrations at the surface, but the other sites showed greater variability after their peak concentrations. In absolute terms, the greatest mean impact period concentrations were found in CM for Cr, Cu, Mn, Ni, V and were identical at CM and HBP for As. HBP had the highest concentration of Pb, Ti and Zn while TWEE had the highest concentrations of Hg and S.

When sediment accumulation rates (SAR) were used to calculate fluxes of trace elements, a much more consistent picture of increasing inputs from baseline to impact periods was revealed (Table 2). Independent sample *t*-tests showed that in both sites, there was a highly significant increase ($p < 0.05$ at CM, $p < 0.01$ at HBP) in almost all 12 elemental fluxes with the only exception being for S at HBP. Excluding Hg and S (see below), much greater proportional increases in fluxes were found at HBP, ranging from 184 % (V) to 303 % (As), i.e. an approximately 3–4 fold increase from baseline (Table 2). At CM, metal fluxes increased by between 73 % (Ti) and 149 % (Zn) but the range was much more comparable for the three elements showing the largest concentration increases in both sites (Cr, Pb and Zn, range 137–149 % increase in flux). While As did not show a significant increase in concentration at CM, the increase in flux was statistically significant, at 120 %. As indicated previously, variations in sediment focusing effects between the three sites appear to be very minor and hence the differences in elemental fluxes described above are likely to reflect real differences in contaminant delivery between sites.

Although proportional increases in fluxes were generally much higher at HBP, the difference in absolute flux values between sites were more muted (Table 2). Likewise, concentration differences between sites were relatively small, indicating that differences in fluxes between sites were largely driven by changes in SAR, which were much greater on average at HBP during the impact period.

4.2.2. *Threshold effects concentrations (TECs) and probable effects concentrations (PECs)*

Despite the clear trends in several trace elements associated with fossil fuel combustion in this global emissions hotspot, the levels of sediment contamination are relatively minor compared with other heavily industrialised regions of the world. Only five elements (As, Cr, Cu, Ni and Zn) show maximum concentrations exceeding consensus sediment quality guidelines, defined as the threshold effects concentration (TEC), below which biological effects would rarely be observed, or the Probable Effects Concentration (PEC), above which detrimental biological effects due solely to a particular contaminant might be expected (MacDonald et al., 2000; Burton Jr., 2002; Canadian Council of Ministers, no date; Table 2; Table S7). Of these, Cr showed the greatest increase to exceed the PEC of 90 µg g^{-1} in all three sites during the impact period, with similar mean (127–147 µg g^{-1}) and peak (140–177 µg g^{-1}) concentrations across sites. However, baseline Cr concentrations at CM and HBP already exceeded the PEC value of 90 µg g^{-1} so it is likely that natural geological sources are present, with additional inputs from fossil fuel combustion increasing concentrations further above the PEC in all sites. Mean concentrations of Cu during the impact period exceeded the TEC of 35.7 µg g^{-1} in CM and TWEE while peak concentrations exceeded the TEC at all sites. However, Cu showed no significant change in CM and a significant decrease in HBP from baseline to impact periods, so power station emissions are unlikely to be the major source.

For Ni, both baseline (CM, HBP) and impact period (all sites) concentrations greatly exceeded the TEC of 18 µg g^{-1} and slightly exceeded the PEC of 36 µg g^{-1}. Hence natural geological sources of Ni must be present in the catchments and inputs from fossil fuel combustion are very minor; only HBP shows a significant but small increase of 5 % from the baseline period. For Zn and especially Pb it is only anomalous peak concentrations (131 and 395 µg g^{-1} respectively) near the surface of CM that exceed the TEC or PEC, so the significant mean increases observed in both CM and HBP, most likely due to power station emissions, are not likely to lead to toxic effects. Despite the greatest proportional increases being found for Hg, which more than doubles in CM from the baseline to impact period, concentrations are all well below the TEC of 170 ng g^{-1}. Trends in Hg concentrations, fluxes and emissions are compared with those for S, N and SCPs below.

4.3. *Mercury, sulphur, nitrogen and SCP trends*

Mercury, S and N have a strong association with emissions from coal-fired power stations and emission estimates back to the 1920s are available for South Africa (Masekoameng et al., 2010; Pretorius et al., 2015; Garnham and Langerman, 2016; Rose et al., 2020). Hence they are considered separately here for comparison of sediment concentrations, fluxes and emission trends. Since SCPs are generated exclusively by high

temperature combustion of coal-series and oil fuels, they are also compared here with Hg, S and N trends.

4.3.1. Mercury

Sediment concentrations of Hg show the greatest proportional increases of all trace metals at both CM and HBP, with an increase of 123 % and 38 % respectively from the baseline to the impact periods (Table 2). At CM the flux of Hg also shows the greatest increase of all trace metals (355 %) while at HBP the opposite is true, with an increase in Hg of only 112 % in the impact period, compared with 184–303 % increases in other trace metals.

Mercury concentrations in all sites show some background variability but a steep increase from the 1980s closely mirrors the increases in Hg emissions from coal-fired power stations (Fig. 4). All three sites show a highly significant correlation between Hg concentrations and emissions (CM, $r = 0.895$, $p < 0.001$; HBP, $r = 0.890$, $p < 0.001$; TWEE, $r = 0.971$, $p = 0.001$). In HBPA Hg concentration varies in the range 22–29 ng g^{-1} until the 1980s, after which there is around a doubling to a peak of 52 ng g^{-1} in around 2015/16. Core CM1 shows greater pre-industrial variability in the range 15–42 ng g^{-1} until the 1980s, increasing to a peak of 77 ng g^{-1} in 2015 after which there is a decline to 51 ng g^{-1} at the surface. For TWEE1 the record only extends back to 1975 when the Hg concentration was 69 ng g^{-1} with a steep increase to a peak of 119 ng g^{-1} at the surface. While the trend in TWEE1 closely matches the other two sites over the common time period, concentrations are much higher – more than double those in HBPA and around 50 % higher than CM1 (Fig. 4a). All sites track the increase in Hg emissions from the 1970s, with Hg concentrations peaking after 2010.

Differences between sites may be due to differences in sediment accumulation rates, so Hg fluxes to the sediment (calculated as the product of concentration and SAR) are presented for comparison in Fig. 4b. Apart from a single sample outlier at HBPA in 1913 (linked to a local peak in SAR), Hg fluxes in CM1 and HBPA are very similar, increasing from background levels of <0.5 ng cm^{-2} yr^{-1} to maxima of >7 ng cm^{-2} yr^{-1} around 2015. Fluxes of Hg in all sites track the increase in emissions even more closely than concentrations (Fig. 4b). All sites show a highly significant correlation between Hg fluxes and emissions (CM, $r = 0.877$, $p < 0.001$; HBP, $r = 0.812$, $p < 0.001$; TWEE, $r = 0.923$, $p < 0.003$).

Interestingly there is a slightly increasing trend in Hg fluxes from the end of the 1800s even prior to the onset of local emissions from power stations. This may reflect long-range sources from elsewhere in the world (cf. Wan et al., 2022; Yang et al., 2023), and/or regional Hg emissions from other anthropogenic sources such as gold mining (which used the mercury amalgam extraction method when it first started in 1886 in the Witwatersrand; Naicker et al., 2003) or biomass burning (Fitzgerald and Lamborg, 2014; Fisher et al., 2023). As with concentrations, Hg fluxes in TWEE1 are much greater than the other sites, increasing from 5.7 ng cm^{-2} yr^{-1} in 1975 (compared with c.2 ng cm^{-2} yr^{-1} in the other sites at that time) up to a peak of around 12.1 ng cm^{-2} yr^{-1} within the last decade, with a mean of 9.76 ng cm^{-2} yr^{-1} for the impact period, around double the figure for the other sites. Despite the clear evidence of increasing Hg inputs into all sites, none of the samples approach the TEC value for Hg in sediment of 170 ng g^{-1} (Burton Jr., 2002).

4.3.2. Sulphur

Sulphur dioxide emissions data show a slow increase from the 1920s followed by a rapid increase in the 1970s to a peak in 2008, after which there has been a small decline (Fig. 4). While sediment sulphur concentration and flux profiles may be affected by post-deposition processing and diagenesis e.g. through changing redox conditions, sediment concentrations of S in TWEE and CM closely track SO_2 emissions with an exponential increase from the 1970s to the 1990s, but in CM there is a large decline from a peak around 1996 to the surface which is linked to sediment accumulation rates (see below). Conversely, TWEE shows the most rapid increase in sediment S concentration between 2001 and 2009, with variability thereafter but a peak in 2015. In HBP there is a much weaker trend in S concentrations but a large peak at the surface. All three sites show a significant correlation between S concentrations and SO_2 emissions (CM, $r = 0.876$, $p < 0.001$; HBP, $r = 0.438$, $p = 0.022$; TWEE, $r = 0.888$, $p < 0.001$). Trends in S concentrations are similar to Hg for all three sites, with much higher concentrations and steeper increases found in CM and TWEE compared with HBP (Fig. 4a).

Taking into account SAR, fluxes of S across sites show a much more consistent pattern than concentrations in tracking SO_2 emissions, albeit with differences between sites in the size of the response (Fig. 4b). All three sites show a highly significant correlation between S fluxes and SO_2 emissions (CM, $r = 0.974$, $P < 0.001$; HBP, $r = 0.490$, $p = 0.010$; TWEE, $r = 0.853$, $p < 0.001$). Both CM and TWEE show rapid increases from the 1970s with peaks in S fluxes around 2009 which closely correspond with the 2008 peak in SO_2 emissions, especially given the error bars on the ^{210}Pb dates. Thereafter, both sites show variability but a levelling off in fluxes, similar to emissions. Although the trend in HBP is much more muted, there is a slight increase in S fluxes from the 1970s but a sharp peak at the surface (Fig. 4b). The much greater similarity between S fluxes and emissions at CM compared with concentrations illustrates the importance of sediment accumulation rates, as also seen with Hg; major increases in SAR can act to dilute concentrations but have a smaller impact on fluxes.

Of all the elements analysed in this study, S showed by far the largest proportional increase in both concentrations (1473 %, $p < 0.001$) and fluxes (2595 %, $p < 0.0001$) from the baseline (pre-1900) to the impact period in CM (Table 2). However, changes in HBP were much smaller and not statistically significant. TWEE showed the greatest concentrations and fluxes of S but the sediment record only goes back to 1975 so there is no pre-industrial baseline for temporal comparison.

4.3.3. Nitrogen and $\delta^{15}N$

Emissions of NO_x follow a near identical trend to SO_2 emissions, increasing rapidly from the 1970s to a peak in 2008. In lake sediments, N is not generally considered to be a conservative element and may be affected by sediment diagenesis as well as local pollution sources and nutrient inputs. Nevertheless, sediment N concentration data for CM1 (the only site with available data) do show a rapid increase from the 1970s to the surface, coincident with the trend in NO_x emissions except for the last few years of the record (Fig. 4a). Although fluxes of N in sediment also show an increase, this only accelerates in the last 20 years of the record while NO_x emissions started to increase much earlier. Hence it can be concluded that sediment N concentrations and fluxes both show increases over the same time period as increasing atmospheric NO_x emissions since the 1970s, but the relationship is much less clear than for Hg and S, given the potentially greater mobility of N in aquatic systems and the wide range of other potential sources. The $\delta^{15}N$ data for CM show some background variability but a slow general increase to a peak in 1978 ($\delta^{15}N = 6.4$ ‰) followed by a rapid decline to a minimum of 4.6 ‰ in 2007, after which there is a rapid increase again to the surface.

4.3.4. SCPs

SCPs first appear in the sediment record at CM and HBP in the 1920s, with a sharp increase in concentrations from the 1940s to a first peak in 1983 (Fig. 4a). From the peak concentration of around 2400 gDM^{-1} in 1983 at CM there is a second peak in 2006 and a decline towards the present but a smaller peak again in the surface sample (c. 1600 gDM^{-1}). A very similar pattern is seen in HBP with SCPs appearing in the sediment record in the 1920s, increasing steeply to a first peak in 1983, although in this case a higher peak concentration occurs (1910 gDM^{-1}) around 2007 before a decline to the surface. At Tweelingspan, the record only goes back to the 1970s so SCPs are found throughout the core. There is a similar sharp increase in SCP concentrations up to a maximum of over 2900 gDM^{-1} between 2006 and 2010 which corresponds more

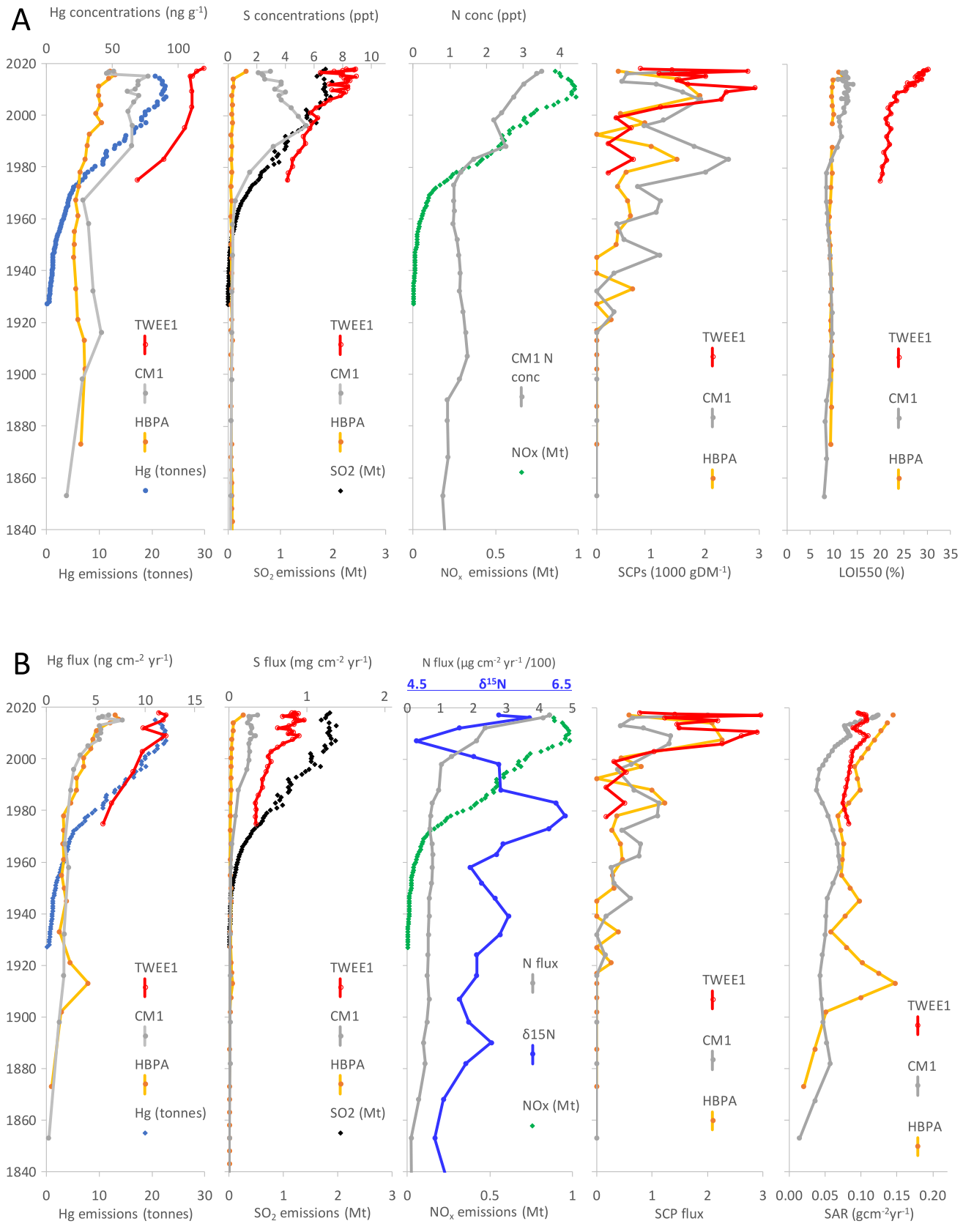

Fig. 4. Annual South African power station emissions of Hg, SO_2 and NO_x (as NO_2), sediment organic carbon (as %LOI550), sediment accumulation rate (SAR) and A) lake sediment concentrations, B) fluxes of Hg, S, N and SCPs (SCP flux $\times 100$ cm^{-2} yr^{-1}).

closely with the second peak seen in HBP (Fig. 4a). For the impact period, mean SCP concentrations are very similar at CM and TWEE (1386 and 1417 gDM^{-1}) but around 50 % higher than HBP (911 gDM^{-1}).

Fluxes of SCPs also show a first peak in 1983 followed by a consistent second peak from 2006 to 2010 in all sites (Fig. 4b). For the impact period, mean SCP fluxes are very similar at CM and HBP (95 and 97 cm^{-2} yr^{-1}) but around 50 % higher at TWEE (137 cm^{-2} yr^{-1}), in contrast with concentrations.

Maximum fluxes reached 201 (in 2017), 227 (in 2008) and 296 (in 2017) SCPs cm^{-2} yr^{-1} in CM, HBP and TWEE respectively.

4.4. Transport climatologies and air mass back trajectories

The transport climatologies (Fig. 5) show the overriding influence of the continental high pressure in controlling airflow over Chrissiesmeer. Flow from the north-east, east and south-east occurs most frequently (around 50 % of the time). Such flow is expected to bring unpolluted air over Chrissiesmeer, unless polluted air originating over the southern African subcontinent is recirculated back over the region. Tyson et al. (1996) have demonstrated that recirculation is a persistent feature of the atmosphere over southern Africa. Pollution from the industrial activities, coal-fired power stations and mines on the Highveld will be carried directly over Chrissiesmeer with airflow from the north-west to the south-west. Such westerly flow occurs around 23 % of the time at ground-level, and around 25 % of the time at higher levels in the boundary layer (Table 3).

Table 3
Wind sector allocations (%) for back trajectories arriving at Chrissiesmeer, at 10 m and 1000 m above ground level, between 1950 and 2015. Bold figures indicate wind directions transporting power stations emissions towards the study area.

Wind sector	10 m agl (dry deposition)	1000 m agl (wet deposition)
N	10.1	10.0
NE	18.1	12.3
E	18.7	19.9
SE	15.6	15.8
S	9.3	7.2
SW	**5.3**	**6.0**
W	**9.2**	**9.6**
NW	**8.4**	**9.3**
Unallocated	5.4	9.9

5. Discussion

5.1. Temporal change in contamination

Palaeolimnological records from the three MLD sites show clear evidence of changes in contamination through time, with the greatest increases found for Hg and S concentrations and fluxes which, at all sites, are significantly and highly correlated with Hg and S emissions. Sediment records from two sites (CM and HBP) extend back to the period before coal-fired power stations were constructed in South Africa, providing a comparison of the pre-1900 baseline with a post-1975 impact period. Mercury concentrations increased by 123 % at CM and 38 % at HBP, while S increased by 1473 % at CM but only 24 % (not significant) at HBP. Significant increases were also found for Cr, Zn, Pb and As concentrations which overlapped over the common period of the record back to 1975 in all three sites, peaking after the end of the 1970s and generally showing a recent decline at the surface, especially at CM. For Cr, Pb and Zn, the proportional increases in concentrations were remarkably similar to each other at CM (28 %) while at HBP the increase in Cr (33 %) and As (30 %) was greater than for Pb (12 %) and Zn (13 %). No other elements analysed by XRF showed consistent concentration increases through time at both CM and HBP and proportional changes were all <10 % (Table 2). All these contaminants strongly suggest coal combustion sources, given their presence in South African coals (Wagner and Hlatshwayo, 2005). Furthermore, increases in SCPs, which are only produced by high temperature fossil fuel combustion, are highly consistent with trends in Hg, S and N emissions from major coal combustion sources in South Africa, with minor increases until the 1970s after which emissions increased rapidly to peak around 2008.

While only 3–4 contaminants showed significant increases in concentrations, all trace element fluxes showed a significant increase in CM and HBP, but increases were mostly much greater (3–4 fold) in HBP than in CM (factor of 0.7–1.5), in contrast to concentrations. The greater increase in most trace element fluxes at HBP is driven by larger increases in SAR (197 %), compared with CM (89 %). However, a different picture emerges for the key contaminants Hg and S. At CM, the increase in Hg fluxes (355 %) is greater than all other trace elements, while at HBP the increase in Hg (112 %) is less than all other trace elements. For S fluxes, there is an even more extreme contrast; the increase at CM is by a factor of 27, while at HBP it is a factor of five and is the only element that does not show a statistically significant increase. Hence SAR alone cannot explain the between-site differences and both Hg and S behave differently from other trace elements in terms of their preservation in the sediment record.

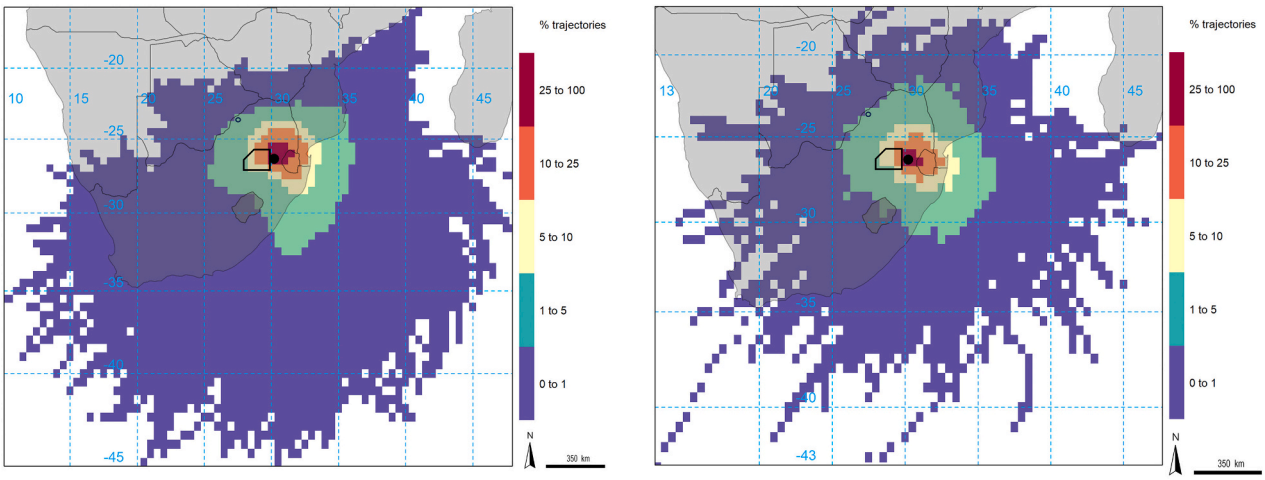

Fig. 5. Back trajectory climatologies for 1950–2015 showing the origin of air at Chrissiesmeer for conditions typical of (left): dry deposition (48-h back trajectories starting 10 m above ground level); and (right): wet deposition (36-h back trajectories starting 1000 m above ground level). Black polygons indicate source regions of emissions.

5.2. Differences in contaminant delivery and preservation between sites

Although the sediment record at TWEE does not extend to the baseline period used for the other sites and therefore cannot be used for temporal comparisons, spatial differences between all three sites for the more recent impact period can be compared. For all elements except Hg and S, concentrations and fluxes at TWEE are generally lower than or comparable to the other two sites (Table 2, Fig. 4). However, concentrations of Hg at TWEE are c. 50 % higher than CM and more than double those in HBP, while concentrations of S are double those at CM and almost 18 times higher than HBP (Table 4). Likewise, Hg fluxes at TWEE are around double the fluxes found at the other two sites, while for S the flux at TWEE is more than double the flux at CM and around 15 times greater than HBP. For SCPs, mean concentrations are very similar at CM and TWEE but around 50 % higher than HBP, while TWEE has roughly 50 % higher SCP fluxes than both of the other sites.

While the reasons for these differences are not immediately apparent given the close proximity of the sites which should preclude major differences in direct regional deposition inputs, two possible factors may offer at least a partial and probably related explanation:

1) hydrologically, TWEE is a much more open system than the other sites as indicated by an EC value which is more than an order of magnitude lower than the other sites (Tables 1, 4) where evaporative processes are much more dominant, suggesting they are more isolated from catchment inputs of contaminants, while re-volatilization is likely to be much more important at the other sites;
2) there are major differences in organic matter content of sediment samples indicated by LOI550 measurements (Fig. 4a), whereby the average OM content of TWEE1 (LOI550 = 24.6 %) is more than double that in CM1 (10.8 %) and HBPA (9.5 %) (Table 4). If deposited Hg is organically bound then this factor alone could explain the much greater fluxes at TWEE, with proportionally lesser impacts on SCP fluxes but greater impacts on S fluxes (see below).

According to Fitzgerald and Lamborg (2014, p.103), "Watersheds are sources of mercury to the aquatic environment. The movement of mercury through watersheds is intimately connected with that of organic matter, especially DOC." Hence both of the above factors may offer possible explanations for the greater sediment fluxes of Hg at TWEE.

Other studies of trends in sediment Hg concentration are very limited in southern Africa. The peak Hg concentration of 119 ng g^{-1} at TWEE is more than double that found in Lake Letšeng-la Letsie (51 ng g^{-1}) in Lesotho by Rose et al. (2020) while the peak in HBP is very similar at 52 ng g^{-1} (Table 2). Fluxes of Hg at Lake Letšeng-la Letsie peaked briefly at around 9 ng cm^{-2} yr^{-1} when the lake was impounded in the late 1960s but otherwise reached a peak of around 7–7.5 ng cm^{-2} yr^{-1} in sediment surface layers (Rose et al., 2020). Another South African study at Mountain Lake in the Eastern Cape (Curtis et al., 2023), some 400 km from the present study, found a peak Hg concentration of 96 ng g^{-1} and flux of 7.9 ng cm^{-2} yr^{-1} at the surface, which are in between the values found at HBP and TWEE. According to Garnham and Langerman (2016) there was a slight decline in Hg emissions from 2011 to 2015 with further reductions expected over subsequent years; this decline is broadly consistent with Hg fluxes found in the current study sites although slightly lagging behind emissions reductions.

The concentrations and fluxes of Hg are within the range of industrialised locations in other parts of the world as well as some relatively remote sites in north China (Wan et al., 2022). In western North American and Central American lake sediments, Hg accumulation rates were found to have increased on average by a factor of 4 (range 2–5) from 1850 to 2000 (Drevnick et al., 2016; Yang et al., 2023), comparable with c. 4.5 in CM (355 %, Table 2). If we assume there are no differences in impact due to sediment focusing for MLD lakes, pre-industrial fluxes are within the range of the global background of 0.2 ng cm^{-2} yr^{-1} and the North American average of 0.7 ng cm^{-2} yr^{-1} (Drevnick et al., 2016) while recent peak fluxes of 7–12 ng cm^{-2} yr^{-1} are much higher than the North American average of 1.9–2.7 ng cm^{-2} yr^{-1} and fall within the range of lakes impacted by mining activities within their catchments or volcanic sources in Central American lakes (Yang et al., 2023).

For S, the differences between sites, as for Hg, may be linked to catchment hydrology, the relative importance of wet versus dry deposition processes and the differences in sediment organic matter, since S can also be organically bound. At HBP it is also known that this very shallow site (max depth 0.4 m at the time of coring) undergoes periodic dessication which could result in the oxidation and/or remobilisation of deposited S. Russell (2008) studied the geochemical evolution of pans in the MLD and proposed that periodic dessication and wind removal of salts accumulated around the dried perimeter through capillary efflorescence could be an important mechanism for transporting salts out of the pans. Wind blowouts during the windiest month of September have been reported by local farmers (Russell, 2008). Russell (2008) also noted that HBP was unique in having nodules containing barite (barium sulphate) accumulated around the perimeter. On the basis of depth, bathymetry and evidence from historic Google Earth imagery, the relative inter-annual change in surface area of HBP is much greater than at CM and TWEE, suggesting a greater role for such dessication and blowout mechanisms at HBP.

Furthermore, another possibly important process leading to differences between sites is fog deposition, shown by Singer et al. (1999) to lead to salt efflorescence on vegetation in the nearby Ermelo area, primarily of the minerals thenardite, bloedite, gypsum and kieserite, all sulphate minerals. These powdery salt crystals were found to be easily dislodged from vegetation and highly soluble; Singer et al. (1999) therefore hypothesized that rain events following such salt accumulation would lead to rapid inwash into pans. Such a mechanism would have a much greater impact on pans with greater C:L ratios (Table 1) and greater surface runoff and could therefore explain the greater fluxes of S at CM and especially TWEE compared with HBP.

NO_x emissions from South African power stations tend to be slightly enriched in ^{15}N but nitrate and ammonium in rainfall (wet deposition) are depleted in ^{15}N, with lower values in summer (Heaton, 1986, 1987). Likewise, biomass burning and vehicle emissions tend to be depleted in ^{15}N (Heaton, 1987, 1990) but nutrient inputs from livestock and sewage are highly elevated in ^{15}N (Kendall et al., 2007). Interestingly, Russell (2008) reported a newspaper article from 2007 voicing local outrage at sewage discharges into Chrissiesmeer (https://www.netwerk24.com/beeld/suid-afrika/nuus/meer-chrissie-n-ramp-kenner-20100617), while subsequent spillages have also been reported in the media, e.g. March 2015 (https://www.youtube.com/watch?v=EabunIMqGFs; https://infrastructurenews.co.za/2015/03/24/task-team-to-investigate-sewage-spillage-in-chrissiesmeer/). These spillages coincide with the period of increasing $\delta^{15}N$ following a major decline in the previous 30

Table 4
Ratios of contaminant concentrations, fluxes and drivers standardised to HBP for the post-1975 impact period.

Site	C:L Ratio	Max Depth	EC	OM	SAR	Concentrations			Fluxes		
						Hg	S	SCP	Hg	S	SCP
TWEE	9.5	6	0.06	2.5	0.9	2.7	17.8	1.5	2.2	14.6	1.4
CM	2.0	3.3	1.37	1.2	0.7	1.6	8.7	1.6	1.1	5.6	1.0
HBP	1	1	1	1	1	1	1	1	1	1	1

years which may be associated with power station emissions, while N fluxes into the sediment also show a rapid increase from 2007 which would be consistent with sewage inputs into the lake. Hence it is possible that the $\delta^{15}N$ profile in CM reflects slowly increasing agricultural and urban inputs from the town of Chrissiesmeer which increase sediment $\delta^{15}N$, followed by a period of rapidly increasing NO_x emissions and wet deposition of N (the dominant component of total N deposition in this part of the Highveld; Collett et al., 2010) from the Highveld power stations (decreasing $\delta^{15}N$ from 1978 to 2007). A second period of rapidly increasing nutrient inputs and $\delta^{15}N$ could then be associated with sewage spills into the lake from the town of Chrissiesmeer. It is also possible that the rapid increase in SAR observed in Chrissiesmeer may be driven by nutrient inputs, especially sewage inputs over at least the last decade.

The greater hydrological connectivity of TWEE with its catchment, as discussed for Hg and S above, could account for the greater SCP fluxes relative to the other two sites. Both peak concentrations and fluxes of SCPs correspond with the period when (or shortly after) emissions of Hg, SO_2 and NO_x peaked in 2008. The second peak in SCP concentrations and fluxes corresponds with the recommissioning of the closest coal-fired power station at Camden, around 30 km south-west of the study sites, between 2005 and 2008, which had previously been mothballed between 1990 and 2005.

The SCP concentrations found in the MLD sites are more than double those found in Lake Letšeng-la Letsie, Lesotho (peak of 900 gDM^{-1}) by Rose et al. (2020) and higher than those reported for Mountain Lake (Eastern Cape of South Africa, peak of 1273 gDM^{-1}) by Curtis et al. (2023). SCP fluxes in the MLD lakes were also around 2–3 times higher than Mountain Lake (peak 111.4 cm^{-2} yr^{-1}), but only 30–100 % higher than Lake Letšeng-la Letsie, Lesotho (peak 148 cm^{-2} yr^{-1}). However, compared with concentrations and fluxes in other industrialised parts of the world (e.g. Rose et al., 1999; Rose and Monteith, 2005; Rose, 2015) SCP contamination in these South African lake sediments is low. Higher fluxes of SCPs might be expected in the MLD lakes given their much closer proximity to the Highveld coal-fired power stations, although the roles of catchment hydrology and rainfall may also contribute to these differences.

5.3. *Effects of organic matter content and sedimentation rates on pollutant concentrations and fluxes*

Increasing pollutant fluxes into lakes do not necessarily indicate increasing atmospheric inputs, but may also reflect increasing inputs from terrestrial catchments, for example through increasing erosional inputs caused by changing land-use or climate change (e.g. Yang et al., 2023). Sediment accumulation rates may likewise reflect either increasing catchment inputs or increasing in-lake production of organic matter. In this study there are clear differences between study sites in terms of OM content of sediments, but spatial differences in SAR are more muted (Fig. 4b).

In considering temporal changes in elemental concentrations and fluxes in sediments at the study sites, the roles of organic matter content and changing SAR must be taken into account. The association of certain contaminants with organic matter has already been noted and proposed as a possible explanation for greater fluxes of Hg and S into TWEE, due to its much greater LOI550. There were no significant differences in LOI550 between HBP and CM in baseline samples but significant differences between all sites (independent samples Kruskal-Wallis; $p < 0.05$) in the impact period.

Significant increases in As, Cr, Pb and Zn concentrations during the impact period correspond with a significant increase in LOI550 (organic matter) at CM (43 %, $p < 0.05$) but not at HBP (6 %, ns). Greater proportional increases at CM for these trace elements (22–28 %) may be driven partly by the greater increase in organic matter at this site, compared with HBP (12 % for Pb and 13 % for Zn) but cannot explain a greater increase in As (30 %) and Cr (33 %) at HBP. For Hg, increases of 123 % at CM and 38 % at HBP cannot be driven solely by increasing OM. Increasing SARs at these sites have clearly not diluted inputs of these contaminants sufficiently to offset increasing concentrations.

The impact of changing SARs on contaminant fluxes is however much more apparent. At HBP, SAR increased by a factor of three from the baseline to impact period, while fluxes of As, Cr, Pb and Zn increased by a factor of 3–4 and Hg by a factor of just over two. At CM, although not significant, mean SAR increased by a factor of around two, while As, Cr, Pb and Zn fluxes increased by a factor of 2–3, and Hg increased by a factor of 4.5. While increasing SAR does therefore clearly contribute to increasing contaminant fluxes, the proportional increases in contaminant fluxes exceed those of SAR, indicating additional sources which are assumed to be direct atmospheric inputs. Hg increases by more than SAR at CM but less than SAR at HBP. In absolute terms though, fluxes of Hg are very similar at CM and HBP for the impact period. The greatest OM content and Hg fluxes were found at TWEE which has SARs in between those of CM and HBP.

For S, concentration in CM increased more than fifteen-fold from baseline to impact period, while OM increased by only 43 % (both $p < 0.05$). At HBP, an apparent 24 % increase in S concentration was not significant, while OM likewise showed a minor and non-significant increase of only 6 %. For the common impact period at TWEE, both OM content (LOI550) and S concentration were more than double the values at CM ($p < 0.05$) and 2.5 (OM) to 18 (S) times higher than at HBP (Table 4). SAR showed a very different relationship between sites and S fluxes. At CM, S fluxes increased >25-fold while SAR less than doubled. At HBP, S fluxes increased five-fold but SAR only tripled. For the common impact period, S fluxes at TWEE were more than double those at CM and almost 15 times greater than at HBP.

Hence while it is clear that both OM content and SAR influence concentrations and fluxes of certain contaminants, especially those which may bind with OM such as Hg and S, the changes in OM and SAR are insufficient by themselves to explain the temporal and spatial patterns observed in MLD lakes. The strong and highly significant correlations between fluxes and power station emissions for Hg and S as well as with SCPs provides very compelling evidence for an over-riding influence of fossil fuel derived sources on contaminant trends in MLD sediments.

5.4. *Why are contaminant levels in MLD lakes near a global emissions hotspot relatively low, in a global context?*

Given the context of the study area and its location very close to a global emissions hotspot (Wenig et al., 2002; Collett et al., 2010; Lourens et al., 2012; Greenpeace, 2018; Myllyvirta, 2021; Sguazzin, 2021), these results show relatively low levels of contamination compared with similar studies in industrialised areas of the northern hemisphere. Although six elements have peak values that exceed sediment TEC or PEC, two (Cu, Ni) appear to be mainly linked to natural geological sources rather than fossil fuel combustion, given their exceedance during the baseline period before 1900 and minor changes through the period of increasing power station emissions. Interestingly, a study of trace metals in soils around a Highveld power station also indicated very elevated natural background levels of Cu, Ni and Mn (Dalton et al., 2018), with no evidence of additional contamination linked to the power station. In our study, single peak values for Pb and Zn which exceed the PEC and TEC at CM may be due to sewage and wastewater contamination in recent years (see above) rather than power station emissions. Peak concentrations of As slightly exceed the TEC at CM and HBP, but mean values are below the TEC. Only Cr shows convincing evidence of increasing concentrations caused by power station emissions which result in an average exceedance of the PEC during the impact period, despite the presence of natural sources which mean that even the baseline concentrations exceeded the PEC. Although Hg showed much greater proportional increases than these other contaminants, there was no exceedance of the TEC at any time during the sediment record.

At least three factors may account for the relatively low levels of contamination recorded in the sediments of MLD lakes and are explored in more detail below:

1. low levels of contaminants in South African coal relative to more polluted regions elsewhere;
2. transport of pollutants away from the study area leading to relatively low local deposition levels; and
3. poor preservation of contaminant records in MLD lakes compared with cooler and wetter regions elsewhere.

5.4.1. Emissions abatement and composition of South African coal

In comparing emissions and deposition of trace elements from coal fired power stations between Mpumalanga and other parts of the world, differences in coal composition and abatement technology must be considered. While particulate matter (PM) emission controls have been installed in all of these power stations, they lack emission control for SO_2 (Kolker et al., 2014). Depending on the PM emission control measures used, removal of some trace metals may vary between 10 and 50 % (Dabrowski et al., 2008; Garnham and Langerman, 2016; Rallo et al., 2012; Zerizghi et al., 2022). The absence of coal-washing of most coal used and relatively lax emissions controls compared with global best practice (Zerizghi et al., 2022) are therefore unlikely to explain the relatively low levels of contamination in the MLD. However, Garnham and Langerman (2016) analysed Hg emissions from all South African coal fired power stations and found the lowest Hg emissions from those located in eastern Mpumalanga (closest to the MLD) while the greatest emissions by far occurred at Lethabo (Free State, south of Johannesburg) and Matimba (Waterberg of Limpopo Province) power stations, furthest from the MLD.

In the global context, South Africa may benefit from cleaner coals relative to other parts of the world – for example Falcon (1986) and Wagner and Hlatshwayo (2005) reported that Permian coals of the southern hemisphere may contain lower concentrations of sulphur and certain trace elements than Carboniferous coals of the northern hemisphere. Local studies of Highveld coal composition indicated lower content of S and trace metals than the global average; for example, Pb in South African coals is only around half the global average (Wagner and Hlatshwayo, 2005; Bergh, 2013; Zerizghi et al., 2022). Leaded gasoline was a major source of national Pb emissions until it was largely replaced by unleaded fuels since 2007 (DoE 2017, in Zerizghi et al., 2022) and so would have declined from around the same time as power station emissions. Interestingly, Wagner and Hlatshwayo (2005) found that South African coals, especially those from the Highveld, contained generally lower concentrations of As, Cu, Pb and Zn (among others) than the global average, while Ni and V were comparable to the global average. The main exceptions in their study, exceeding the global average, were Cr and to a lesser degree Hg, which is entirely consistent with the major coal-associated contaminants found in MLD lake sediments. The highest concentrations of Pb and Hg in South African coals were generally found in the Waterberg coals (Wagner and Tlotleng, 2012; Bergh, 2013) where two of the largest emitting power stations are also located (Garnham and Langerman, 2016). Hence it is possible that lake sediment studies there may record higher levels of Pb and Hg contamination than the Highveld sites.

5.4.2. Fate of power station emissions

Prior to this study, it was assumed that the lakes of the MLD would experience high deposition loads of fossil-fuel derived contaminants because of their proximity to a large number of coal-fired power stations on the Mpumalanga Highveld. Earlier air pollution modelling studies (e.g. Bruwer and Kornelius, 2017; Diab et al., 2004; Freiman and Piketh, 2003; Zunckel et al., 2000) suggest that pollutants emitted on the South African Highveld are predominantly exported to the east and should therefore greatly affect atmospheric deposition at Chrissiesmeer. Although clear evidence of sediment contamination trends tracking the increase in coal combustion has been shown, pollution levels are relatively low compared with similar studies from the northern hemisphere.

One contributing factor may be the strong seasonal variation in rainfall and prevailing winds found in the study region. Russell (2008) summarised earlier geomorphological studies indicating that the morphology of many pans in the MLD, including Chrissiesmeer, showed a north-south orientation which was perpendicular to the prevailing winds. Inspection of wind rose diagrams for the periods 1993–2007 in that study showed that the prevailing wind directions were easterly during summer but westerly or northerly in winter. Since the MLD is located in the summer rainfall zone of South Africa, then most rainfall occurs when easterly winds are blowing power station emissions to the west, away from the MLD. Hence wet deposition inputs to the MLD lakes would be minimal compared with dry deposition inputs. Back-trajectory modelling using HYSPLIT in the current study (Fig. 5, Table 3) corroborates these findings; easterly wind directions are twice as frequent as westerly winds, indicating that for most of the year, pollutants are being transported away from the MLD lakes without the polluted air masses passing directly over the study sites. These easterly winds are more frequent in summer, meaning that washout of atmospheric pollutants from power stations in wet deposition is minimal in the study area. However, there could be an accumulation of some pollutants in efflorescence through fog deposition during the dry winter months (Singer et al., 1999) which may result in a sudden influx event into lakes during the first rains of the wet season.

An additional factor may simply be the exponential decline in atmospheric deposition of contaminants with distance from source, as found in similar studies elsewhere, for example in the Athabasca Oil Sands region of Canada (Kelly et al., 2010; Curtis et al., 2010; Cooke et al., 2017). Kelly et al. (2010) used a distance of 50 km to distinguish between higher levels of “near development” (source) contamination and “background” levels of contaminants at distances of >50 km, while Curtis et al. (2010) found the greatest evidence for Hg contamination and acidification in the site closest to the centre of oil sands processing activities, at c.50 km distance. In our study, only one power station (Camden, at 35 km) lies within 50 km and indeed the patterns in trace metal and SCP concentrations and fluxes in sediments reflect the operation, mothballing and recommissioning of this site (Fig. 4; Table S1). However, the presence of another five power stations within 50-100 km and a total of 13 within 230 km must contribute significantly to “background” deposition, given that the South African Highveld itself constitutes the major emissions hotspot for the entire southern hemisphere.

5.4.3. Importance of hydrology and hydroperiod

Depressional wetlands or pans are generally characterised by a lack of surface hydrology, suggesting that the main pathways for pollutant inputs are via groundwater and throughflow or by direct deposition to lake surfaces from the atmosphere. The differences in contaminant concentrations and fluxes found in the three study sites despite their very close proximity to each other in the context of regional pollution sources most likely reflects their widely differing catchment: lake surface area ratios as well as the presence of seasonal or ephemeral surface flows, as indicated by the presence of stream channels and seepage wetlands on 1:50,000 maps and visible on Google Earth imagery. TWEE is the only one of the study sites with a surface outflow stream and a very low EC (salinity) compared with the other sites, indicating a much greater ratio of inflow to evaporation. Unfortunately the short sediment record from this site did not extend to the baseline period pre-1900 but the data show much higher concentrations and fluxes during the impact period (post-1975) of Hg and S, but not for other trace elements, possibly reflecting differences in wet and dry deposition pathways between contaminants. In particular, contaminants strongly associated with organic matter (Hg, S) show a larger signal in TWEE where the sediment organic content (assessed as LOI550) is much greater than in the other

sites.

Hydroperiod and seasonal or inter-annual variations in hydrology are also important for preserving contaminant records in sediments. Depressional wetlands in the MLD have been classified as permanently, seasonally, or intermittently inundated (Van Deventer et al., 2022) with the weakest contamination signal found in the only non-permanent site, HBP. Even the largest lakes in the MLD are known to have dried out on occasion: Wellington (1943) states that local farmers recorded Chrissiesmeer to have dried out in 1901–03 and again in 1933, while according to Trevor (1906) Chrissiesmeer was sometimes dry between 1903 and 1906. Tarboton (2009) indicated that Chrissiesmeer has dried out five times in the past century, with the most recent occurrence recorded in 1993–94. Chrissiesmeer is by far the largest of the study sites by volume and area, with a maximum depth of 1.3 m at the time of coring, compared with 2.5 m in TWEE and only 0.4 m in HBP. The study of Van Deventer et al. (2022) indicated that both CM and TWEE were largely perennial (permanently inundated) whereas HBP varies between permanent and seasonal inundation from year to year. Wellington (1943) records the HBP pan (Driefontein pan "FF" in his study) as being dry in 1942. Hence the potential removal of pollutants through desiccation and blowout is likely to be much more important at HBP than the other sites.

6. Conclusions

According to Zerizghi et al. (2022), South Africa is ranked fourth globally in terms of power station SO_2 emissions and related health impacts. The presence of 11 coal-fired power plants and the SASOL Secunda Plant within 150 km indicates that the MLD is located close to a global hotspot of fossil-fuel associated emissions. Sediments of the three pans studied show clear evidence of contamination, with concentrations and fluxes of fossil-fuel derived contaminants such as Hg, S and Cr as well as SCPs tracking historical emissions of Hg, S and NO_x linked to coal combustion. Hence our first hypothesis (H1) is strongly supported.

However, contamination is lower than anticipated, with Cr being the only emissions-related trace element exceeding the PEC, due to its relatively high concentration in coal measures mined and burnt on the Highveld. For many of the other potentially toxic trace elements associated with power station emissions in other parts of the world, the lakes of the MLD are relatively lightly impacted due to the fortunate combination of low contaminant levels in local coals, regional climate and hydrology. Our second hypothesis (H2) is therefore largely refuted, with only minor levels of contamination, on average mostly below the minimum threshold for ecological concern (TEC), in the context of industrialised regions globally.

Our third hypothesis (H3) that similar regionally-derived contaminant records would be found in all three closely co-located sites is only partially supported. While all three sites show consistent trends, they record varying absolute levels of contamination as indicated by trace element concentrations and fluxes, due to differences in both pollutant delivery and preservation in the sediment record driven largely by differences in surface hydrology and hydroperiod.

The future environmental impact of power station emissions on the unique lakes and pans of the MLD is uncertain. Although emissions have declined slightly since peaking around 2008 in South Africa, coal will remain the dominant energy source for the foreseeable future. Zerizghi et al. (2022) suggest that the practice of using low-grade coal in South Africa and the decline of good quality coal reserves, along with an ageing fleet of coal-fired power stations, could lead to increasing emissions in future even without any increase in coal consumption. In addition, the impacts of global climate change on regional recirculation patterns and rainfall are poorly understood.

Across a range of climate change downscaling scenarios, increased temperatures of as much as 3 °C by 2040–2060 are projected for Mpumalanga while rainfall projections range from drastic decreases to increases (especially in the Lowveld) associated with more frequent landfall of tropical lows (Department of Environmental Affairs, 2018). The implications of such changes for depressional wetlands and other water bodies in the region suggest an increasing role of evaporative processes but uncertainty in precipitation inputs which may lead to greater hydrological variability and occurrence of extreme events. These changes act to reduce resilience of aquatic ecosystems, making them more vulnerable to impacts from pollution. The differences in pollutant loadings between study sites appear to be largely driven by the balance between intermittent surface runoff and evaporation, so increasing temperatures and possibly more extreme rainfall events will certainly impact on pollutant transport into lakes.

In the context of these uncertainties, our data provide a baseline against which to assess future threats and provide a sound basis for further research. The results have implications for southern African water resource policy, management and conservation and suggest that similar studies should be conducted in other regions where the role of wet deposition of contaminants may be much greater, for example to the west of the power stations clustered on the Highveld, or in the Waterberg area of Limpopo province to the north west.

CRediT authorship contribution statement

C.J. Curtis: Writing – original draft, Visualization, Validation, Methodology, Investigation, Funding acquisition, Formal analysis, Conceptualization. **N.L. Rose:** Writing – review & editing, Visualization, Resources, Project administration, Methodology, Investigation, Funding acquisition, Formal analysis, Data curation, Conceptualization. **H. Yang:** Writing – review & editing, Validation, Formal analysis. **S. Turner:** Writing – review & editing, Validation, Formal analysis, Data curation. **K. Langerman:** Writing – review & editing, Visualization, Methodology, Formal analysis. **J. Fitchett:** Writing – review & editing, Visualization, Project administration, Methodology, Investigation, Funding acquisition, Conceptualization. **A. Milner:** Writing – review & editing, Methodology, Investigation, Funding acquisition, Data curation, Conceptualization. **A. Kabba:** Writing – review & editing, Visualization, Formal analysis. **J. Shilland:** Writing – review & editing, Methodology, Formal analysis.

Declaration of competing interest

The authors declare no competing financial interests.

Data availability

Data will be made available on request.

Acknowledgements

This project was funded by the National Geographic Society grant to NR (Grant Number: CP-124R-17) with additional support to AM from the Quaternary Research Association and Royal Holloway University of London. We are grateful to the NOAA Air Resources Laboratory (ARL) for the provision of the HYSPLIT transport and dispersion model (http://www.ready.noaa.gov) used in this publication. Finally, we would like to thank the local landowners and residents of Chrissiesmeer for permission to access the study sites with boats and coring equipment.

Appendix A. Supplementary data

Supplementary data to this article can be found online at https://doi.org/10.1016/j.scitotenv.2024.173493.

References

Appleby, P.G., 2001. Chronostratigraphic techniques in recent sediments. In: Last, W.N., Smol, J.P. (Eds.), Tracking Environmental Change Through Lake Sediments, Basin

Analysis, Coring and Chronological Techniques, vol. 1. Kluwer, Dordrecht, pp. 171–203.
Appleby, P.G., Richardson, N., Nolan, P.J., 1992. Self-absorption corrections for well-type germanium detectors. Nucl. Instrum. Methods Phys. Res. Sect. B Beam Interact. Mater. Atoms 71, 228–233.
Battarbee, R.W., Shilland, E.M., Kernan, M., Monteith, D.T., Curtis, C.J., 2014. Recovery of acidified surface waters from acidification in the United Kingdom after twenty years of chemical and biological monitoring (1988-2008). Ecol. Indic. 37B, 267–273 (ISSN: 1470-160X).
Bergh, J.P., 2013. South African coals: distribution of trace elements. Inside Min. 10, 12–14.
Birdlife, 2021. https://www.birdlife.org.za/what-we-do/important-bird-and-biodiversity-areas/what-we-do/iba-directory/chrissie-pans (Accessed 09 November 2021).
Bruwer, A.P., Kornelius, G., 2017. Modeling the effects of biogenic NOX emissions on the South African Highveld and Waterberg regions. Water Air Soil Pollut. 228, 326.
Burger, M., van Vuren, J.H.J., de Wet, L., Nel, A., 2019. A comparison of water quality and macroinvertebrate community structure in endorheic depression wetlands and a salt pan in the Gauteng province, South Africa. Environ. Monit. Assess. 191, 14.
Burton Jr., G.A., 2002. Sediment quality criteria in use around the world. Limnology 3, 65–76.
Canadian Council of Minsters n.d. (no date) Sediment Quality Guidelines for the Protection of Aquatic Life Freshwater and Marine ISQG/PEL. https://ccme.ca/en/summary-table (Accessed 13th May 2024).
Carslaw, D.C., 2015. The Openair Manual — Open-Source Tools for Analysing Air Pollution Data. Manual for Version 1.1-4. King's College London.
Carslaw, D.C., Ropkins, K., 2012. openair — an R package for air quality data analysis. Environ. Model Softw. 27–28, 52–61.
Collett, K.S., Piketh, S.J., Ross, K.E., 2010. An assessment of the atmospheric nitrogen budget on the South African Highveld. S. Afr. J. Sci. 106, 1–9.
Cooke, C.A., Kirk, J.L., Muir, D.C., Wiklund, J.A., Wang, X., Gleason, A., Evans, M.S., 2017. Spatial and temporal patterns in trace element deposition to lakes in the Athabasca oil sands region (Alberta, Canada). Environ. Res. Lett. 12 (12), 124001.
Curtis, C.J., Flower, R., Rose, N., Shilland, J., Simpson, G.L., Turner, S., Yang, H., Pla, S., 2010. Palaeolimnological assessment of lake acidification and environmental change in the Athabasca Oil Sands Region of Northern Alberta. J. Limnol. 69, 92–104.
Curtis, C.J., Rose, N.L., Khanzada, T., Turner, S., Yang, H., Humphries, M., 2023. Anthropocene environmental change in an overlooked South African lake: Mountain Lake, Matatiele, Eastern Cape. Trans. R. Soc. S. Afr. 78, 45–66.
Dabrowski, J.M., de Klerk, L.P., 2013. An assessment of the impact of different land use activities on water quality in the upper Olifants River catchment. Water SA 39, 231–244.
Dabrowski, J.M., Ashton, P.J., Murray, K., Leaner, J.J., Mason, R.P., 2008. Anthropogenic mercury emissions in South Africa: coal combustion in power plants. Atmos. Environ. 42, 6620–6626.
Dalton, A., Feig, G.T., Barber, K., 2018. Trace metal enrichment observed in soils around a coal fired power plant in South Africa. Clean Air J. 28, 1–9.
Daniels, S.R., Phiri, E.E., Bayliss, J., 2014. Renewed sampling of inland aquatic habitats in southern Africa yields two novel freshwater crab species (Decapoda: Potamonautidae: Potamonautes). Zool. J. Linn. Soc. Lond. 171, 356–369.
Das, S.K., Routh, J., Roychoudhury, A.N., Klump, J.V., 2008. Major and trace element geochemistry in Zeekoevlei, South Africa: a lacustrine record of present and past processes. Appl. Geochem. 23, 2496–2511.
de Klerk, A.R., De Klerk, L.P., Chamier, J., Wepener, V., 2012. Seasonal variations of water and sediment quality parameters in endorheic reed pans on the Mpumalanga Highveld. Water SA 38, 663–672.
de Klerk, A.R., de Klerk, L.P., Oberholster, P.J., Ashton, P.J., Dini, J.A., Holness, S.D., 2016. A Review of Depressional Wetlands (Pans) in South Africa, Including a Water Quality Classification System. Water Research Commission Report No 2230/1/16. Gezina, South Africa.
Dean Jr., W.E., 1974. Determination of carbonate and organic matter in calcareous sediments and sedimentary rocks by loss on ignition: comparison with other methods. J. Sediment. Petrol. 44, 242–248.
Department of Environmental Affairs, 2018. South Africa's Third National Communication under the United Nations Framework Convention on Climate Change. Republic of South Africa, Pretoria, South Africa (351pp).
Diab, R.D., Thompson, A.M., Mari, K., Ramsay, L., Coetzee, G.J.R., 2004. Tropospheric ozone climatology over Irene, South Africa, from 1990 to 1994 and 1998 to 2002. J. Geophys. Res. 109, D20301.
Draxler, R.R., Hess, G.D., 1998. An overview of the HYSPLIT_4 modeling system of trajectories, dispersion, and deposition. Aust. Meteorol. Mag. 47, 295–308.
Drevnick, P.E., Cooke, C.A., Barraza, D., Blais, J.M., Coale, K.H., Cumming, B.F., Curtis, C.J., et al., 2016. Spatiotemporal patterns of mercury accumulation in lake sediments of western North America. Sci. Total Environ. 568, 1157–1170.
Falcon, R.M.S., 1986. Classification of coals in southern Africa. In: Annhaesser, C.R., Maske, S. (Eds.), Mineral Deposits of Southern Africa, vol. II. Geological Society of Southern Africa, pp. 1899–1921.
Fioletov, V.E., McLinden, C.A., Griffin, D., Abboud, I., Krotkov, N., Leonard, P.J., Li, C., Joiner, J., Theys, N., Carn, S., 2023. Version 2 of the global catalogue of large anthropogenic and volcanic SO 2 sources and emissions derived from satellite measurements. Earth Syst. Sci. Data 15 (1), 75–93. https://doi.org/10.5194/essd-15-75-2023.
Fisher, J.A., Schneider, L., Fostier, A.H., et al., 2023. A synthesis of mercury research in the southern hemisphere, part 2: anthropogenic perturbations. Ambio 52, 918–937.
Fitzgerald, W.F., Lamborg, C.H., 2014. Geochemistry of mercury in the environment. In: Lollar, B.S., Holland, H.D., Turekian, K.K. (Eds.), Environmental Geochemistry (2nd Edition), Treatise on Geochemistry, Elsevier, vol. 11. Oxford, UK, pp. 91–129.
Foster, L., Malherbe, W., Ferreira, M., Van Vuren, J.H.J., 2015. Macroinvertebrate variation in endorheic depression wetlands in North West and Mpumalanga provinces, South Africa. Afr. J. Aq. Sci. 40, 287–297.
Freiman, M.T., Piketh, S.J., 2003. Air transport into and out of the industrial Highveld region of South Africa. J. Appl. Meteorol. 42, 994–1002.
García-Rodríguez, F., Anderson, C.R., Adams, J.B., 2007. Paleolimnological assessment of human impacts on an urban South African lake. J. Paleolimnol. 38, 297–308.
Garmo, Ø.A., Skjelkvåle, B.L., de Wit, H.A., Colombo, L., Curtis, C., Fölster, J., Hoffmann, A., Hruška, J., Høgåsen, T., Jeffries, D., Keller, W., Majer, V., Monteith, D. T., Paterson, A.M., Rogora, M., Rzychon, D., Steingruber, S., Stoddard, J.L., Vuorenmaa, J., Worsztynowicz, A., 2014. Trends in surface water chemistry in acidified areas in Europe and North America from 1990 to 2008. Water Air Soil Pollut. 225, 1880.
Garnham, B.L., Langerman, K.E., 2016. Mercury emissions from South Africa's coal-fired power stations. Clean Air J. 26, 14–20.
Greenpeace, 2018. New satellite data reveals world's largest NO2 air pollution emission hotspots - Greenpeace Media Briefing. https://storage.googleapis.com/planet4-international-stateless/2018/10/07426a79-no2-air-pollution-analysis-greenpeace.pdf.
Grennfelt, P., Engleryd, A., Forsius, M., Hov, Ø., Rodhe, H., Cowling, E., 2020. Acid rain and air pollution: 50 years of progress in environmental science and policy. Ambio 49, 849–864.
Grundling, P., Linström, A., Grobler, R., Engelbrecht, J., 2008. The Tevredenpan peatland complex of the Mpumalanga Lakes District. In: International mire conservation group. Couwenberg, J. and Joosten, H. (2008) Newsletter Issue 2008/1. https://www.imcg.net/pages/publications/newsletter.php. (Accessed 24 January 2024).
Heaton, T.H.E., 1986. Isotopic studies of nitrogen pollution in the hydrosphere and atmosphere: a review. Chem. Geol. Isotope Geosci. Sect. 59, 87–102.
Heaton, T.H.E., 1987. 15N/14N ratios of nitrate and ammonium in rain at Pretoria, South Africa. Atmos. Environ. 21, 843–852.
Heaton, T.H.E., 1990. 15N/14N ratios of NOx from vehicle engines and coal-fired power stations. Tellus B 42, 304–307.
Heiri, O., Lotter, A.F., Lemcke, G., 2001. Loss on ignition as a method for estimating organic and carbonate content in sediments: reproducibility and comparability of results. J. Palaeolim. 25, 101–110.
Huizenga, J.M., Silberbauer, M., Dennis, S.R., Dennis, I., 2013. An inorganic water chemistry dataset (1972-2011) of rivers, dams, and lakes in South Africa. WaterSA 39, 335–339.
Kabba, A., 2019. A Palaeolimnological Assessment of Spheroidal Carbonaceous Particles and Trace Metals in Tweelings Pan, Mpumalanga. Unpublished MSc Dissertation, Dept of Geography, University College London, 69pp.
Kading, T.J., Mason, R.P., Leaner, J.J., 2009. Mercury contamination history of an estuarine floodplain reconstructed from a ^{210}Pb-dated sediment core (Berg River, South Africa). Mar. Pollut. Bull. 59, 116–122.
Kelly, E.N., Schindler, D.W., Hodson, P.V., Short, J.W., Radmanovich, R., Nielsen, C.C., 2010. Oil sands development contributes elements toxic at low concentrations to the Athabasca River and its tributaries. Proc. Natl. Acad. Sci. U. S. A. 107 (37), 16178–16183.
Kendall, C., Elliott, E.M., Wankel, S.D., 2007. Tracing anthropogenic inputs of nitrogen to ecosystems. Chapter 12. In: Michener, R., Lajtha, K. (Eds.), Stable isotopes in Ecology and Environmental Science. Blackwell Publishing, Boston, pp. 375–449.
Kok, L., Van Zyl, P.G., Beukes, J.P., Swartz, J.-S., Burger, R.P., Ellis, S., Josipovic, M., Vakkari, V., Laakso, L., Kulmala, M., 2021. Chemical composition of rain at a regional site on the South African Highveld. Water SA 47, 326–337.
Kolker, A., Senior, C., Van Alphen, C., 2014. Collaborative Studies for Mercury Characterization in Coal and Coal Combustion Products, Republic of South Africa. US Department of the Interior, US Geological Survey Open-File Report 2014–1153.
Korhonen, K., Giannakaki, E., Mielonen, T., Pfüller, A., Laakso, L., Vakkari, V., Baars, H., Engelmann, R., Beukes, J.P., Van Zyl, P.G., Ramandh, A., Ntsangwane, L., Josipovic, M., Tiitta, P., Fourie, G., Ngwana, I., Chiloane, K., Komppula, M., 2013. Atmospheric boundary layer top height in South Africa: measurements with lidar and radiosonde compared to three atmospheric models. Atmos. Chem. Phys. Discuss. 13, 17407–17450.
Kotzé, P., 2011. Hands-on education a hit in biodiversity hotspot: aquatic environment. Water Wheel 10, 30–34.
Kotze, P., du Preez, H.H., van Vuren, J.H.J., 1999. Bioaccumulation of copper and zinc in Oreochromis mossambicus and Clarias gariepinus, from the Olifants River, Mpumalanga, South Africa. WaterSA 25, 99–110.
Lancaster, I.N., 1978. The pans of the Southern Kalahari, Botswana. Geogr. J. 144, 81–98.
Le Maitre, D.C., Seyler, H., Holland, M., Smith-Adao, L.B., Nel, J.L., Maherry, A., Witthüser, K., 2018. Strategic water source areas for surface water (vector data). In: One of the Outputs of the Identification, Delineation and Importance of the Strategic Water Source Areas of South Africa, Lesotho and Swaziland for Surface Water and Groundwater, WRC Report No TT 754/1/18. South Africa, Water Research Commission, Pretoria.
Lourens, A.S.M., Butler, T.M., Beukes, J.P., Van Zyl, P.G., Beirle, S., Wagner, T.K., Heue, K.-P., Pienaar, J.J., Fourie, G.D., Lawrence, M.G., 2012. Re-evaluating the NO2 hotspot over the South African Highveld. S. Afr. J. Sci. 108, 1146 (6 pages).
MacDonald, D.D., Ingersoll, C.G., Berger, T.A., 2000. Development and evaluation of consensus-based sediment quality guidelines for freshwater ecosystems. Arch. Environ. Contam. Toxicol. 39, 20–31.
Masekoameng, K.E., Leaner, J., Dabrowski, J., 2010. Trends in anthropogenic mercury emissions estimated for South Africa during 2000–2006. Atmos. Environ. 44, 3007–3014.

McCarthy, T.S., Venter, J.S., 2006. Increasing pollution levels on the Witwatersrand recorded in the peat deposits of the Klip River wetland. S. Afr. J. Sci. 102, 27–34.
Meteoblue, 2024. Simulated historical climate & weather data for Chrissiesmeer. https://www.meteoblue.com/en/weather/historyclimate/climatemodelled/chrissiesmeer_south-africa_1013563 (Accessed 12th May 2024).
Myllyvirta, L., 2021. Eskom is now the world's most polluting power company. https://energyandcleanair.org/wp/wp-content/uploads/2021/10/Eskom-is-now-the-worlds-most-polluting-power-company.pdf.
Naicker, K., Cukrowska, E., McCarthy, T.S., 2003. Acid mine drainage arising from gold mining activity in Johannesburg, South Africa and environs. Environ. Pollut. 122, 29–40.
Nel, J.L., Colvin, C., Le Maitre, D.C., Smith, J., Haines, I., 2013. South Africa's strategic water source areas. In: CSIR Report CSIR/NRE/ECOS/ER/2013/0031/A. South Africa, CSIR, Stellenbosch.
Pretorius, I., Piketh, S., Burger, R., Neomagus, H., 2015. A perspective on South African coal fired power station emissions. J. Energy S. Afr. 26 (3), 27–40.
Raik, K., 2022. Tracking the effect of pollution deposition from coal-fired power stations over the past 200 years on southern African lakes, using diatoms as a proxy. Unpublished MSc Dissertation, University of the Witwatersrand, 192pp. Available at: https://wiredspace.wits.ac.za/server/api/core/bitstreams/8c904643-6432-4063-9dd1-e461ff9161a1/content (Accessed 19 April 2024).
Rallo, M., Lopez-Anton, M.A., Contreras, M.L., Maroto-Valer, M.M., 2012. Mercury policy and regulations for coal-fired power plants. Environ. Sci. Pollut. Res. 19, 1084–1096.
Renberg, I., Hanson, H., 2008. The HTH sediment corer. J. Paleolimnol. 40, 655–659.
Roffe, S.J., Fitchett, J.M., Curtis, C.J., 2020. Determining the utility of a percentile-based wet-season start- and end-date metrics across South Africa. Theor. Appl. Climatol. 140, 1331–1347.
Rose, N.L., 1994. A note on further refinements to a procedure for the extraction of carbonaceous fly-ash particles from sediments. J. Paleolimnol. 11, 201–204.
Rose, N.L., 2008. Quality control in the analysis of lake sediments for spheroidal carbonaceous particles. Limnol. Oceanogr. Methods 6, 172–179.
Rose, N.L., 2015. Spheroidal carbonaceous fly-ash particles provide a globally synchronous stratigraphic marker for the Anthropocene. Environ. Sci. Technol. 49, 4155–4162.
Rose, N.L., Monteith, D.T., 2005. Temporal trends in spheroidal carbonaceous particle deposition derived from annual sediment traps and lake sediment cores and their relationship with non-marine sulphate. Environ. Pollut. 137, 151–163.
Rose, N.L., Harlock, S., Appleby, P.G., 1999. The spatial and temporal distributions of spheroidal carbonaceous fly-ash particles (SCP) in the sediment records of European mountain lakes. Water Air Soil Pollut. 113, 1–32.
Rose, N.L., Milner, A.M., Fitchett, J.M., Langerman, K.E., Yang, H., Turner, S.D., Jourdan, A.-L., Shilland, J., Martins, C.C., Câmara de Souza, A., Curtis, C.J., 2020. Natural archives of long-range transported contamination at the remote lake Letšeng-la Letsie, Maloti Mountains, Lesotho. Sci. Total Environ. 737, 139642.
Rose, N.L., Turner, S.D., Unger, L.E., Curtis, C.J., 2021. The chronostratigraphy of the Anthropocene in southern Africa: current status and potential. S. Afr. J. Geol. 124, 1093–1106.
Rouault, M., Roy, S.S., Balling Jr., R.C., 2012. The diurnal cycle of rainfall in South Africa in the austral summer. Int. J. Climatol. 33, 770–777.
Russell, J.L., 2008. The Inorganic Chemistry and Geochemical Evolution of Pans in the Mpumalanga Lakes District, South Africa. MSc Geology [Unpublished]. University of Johannesburg.
Sguazzin, A., 2020. The World's Biggest Emitter of Greenhouse Gases: the emissions from Sasol's Secunda plant exceed the individual totals of more than 100 countries. https://www.bloomberg.com/news/features/2020-03-17/south-africa-living-near-the-world-s-biggest-emitting-plant.
Sguazzin, A., 2021. South Africa Power Giant Is Now World's Biggest Sulfur Dioxide Emitter, CREA Says. https://www.bloomberg.com/news/articles/2021-10-05/eskom-is-now-world-s-biggest-sulfur-dioxide-emitter-crea-says#xj4y7vzkg (Accessed 25 January 2024).
Shaw, P., 1988. Lakes and pans. In: Moon, B.P., Dardis, G.F. (Eds.), The Geomorphology of Southern Africa. Southern Book Publishers, Johannesburg, South Africa, pp. 120–140.
Silberbauer, M., 2020. Internet-based applications for interrogating 50 years of data from the South African national water quality monitoring network. Hydrol. Sci. J. 65, 726–734.
Simelane, S.P., Langerman, K.E., 2024. The sensitivity of health impact assessments of PM2.5 from South African coal-fired power stations. Air Qual. Atmos. Health 17, 325–340.
Singer, A., Kirsten, W.F.A., Buhmann, C., 1999. A proposed fog deposition mechanism for the formation of salt efflorescences in the Mpumalanga Highveld, Republic of South Africa. Water Air Soil Pollut. 109, 313–325.
Spratt, J., 2019. A Palaeolimnological determination of a regional industrial signal in the sediments of Mpumalanga Highveld pans. Unpublished MSc Geography Dissertation, Dept of Geography, Archaeology and Environmental Studies, University of the Witwatersrand, Johannesburg, South Africa, 106pp. https://wiredspace.wits.ac.za/items/e449be72-4470-464e-8f72-b1783a825a84.
Stein, A.F., Draxler, R.R., Rolph, G.D., Stunder, B.J.B., Cohen, M.D., Ngan, F., 2015. NOAA's HYSPLIT atmospheric transport and dispersion modeling system. Bull. Am. Meteorol. Soc. 96, 2059–2077.
Tarboton, W., 2009. Motivation for Ramsar Status for the Chrissiesmeer Panveld: Avifauna. Unpublished report. Nelspruit: Mpumalanga Tourism and Parks Agency, 20pp.
Trevor, T.G., 1906. The physical features of the Transvaal. Geogr. J. 28, 50–65.
Tweddle, D., Bills, R., Swartz, E., Coetzer, W., Da Costa, L., Engelbrecht, J., Cambray, J., Marshall, B., Impson, D., Skelton, P.H., Darwall, W.R.T., Smith, K.S., 2009. Chapter 3. The status and distribution of freshwater fishes. In: Darwall, W.R.T., Smith, K.G., Tweddle, D., Skelton, P. (Eds.), The Status and Distribution of Freshwater Biodiversity in Southern Africa. IUCN and Grahamstown, South Africa: SAIAB, Gland, Switzerland, pp. 21–37.
Tyson, P.D., Garstang, M., Swap, R., 1996. Large-scale recirculation of air over Southern Africa. J. Appl. Meteorol. 35, 2218–2236.
Van Deventer, H., Smith-Adao, L., Collins, N.B., Grenfell, M., Grundling, A., Grundling, P.-L., Impson, D., Job, N., Lötter, M., Ollis, D., Petersen, C., Scherman, P., Sieben, E., Snaddon, K., Tererai, F., Van der Colff, D., 2019. South African National Biodiversity Assessment 2018: Technical Report. Volume 2b: Inland Aquatic (Freshwater) Realm. CSIR report number CSIR/NRE/ECOS/IR/2019/0004/A. South African National Biodiversity Institute, Pretoria.
Van Deventer, H., Linström, A., Durand, J.F., Naidoo, L., Cho, M.A., 2022. Deriving the maximum extent and hydroperiod of open water from Sentinel-2 imagery for global sustainability and biodiversity reporting for wetlands. Water SA 48, 75–89.
Venter, A.D., van Zyl, P.G., Beukes, J.P., Josipovic, M., Hendriks, J., Vakkari, V., Laakso, L., 2017. Atmospheric trace metals measured at a regional background site (Welgegund) in South Africa. Atmos. Chem. Phys. 17, 4251–4263.
Wagner, N.J., Hlatshwayo, B., 2005. The occurrence of potentially hazardous trace elements in five Highveld coals, South Africa. Int. J. Coal Geol. 63, 228–246.
Wagner, N.J., Tlotleng, M.T., 2012. Distribution of selected trace elements in density fractionated Waterberg coals from South Africa. Int. J. Coal Geol. 94, 225–237.
Wan, D., Yang, H., Song, L., Jin, Z., Mao, X., Yang, J., 2022. Sediment records of global and regional Hg emissions to the atmosphere in North China over the last three centuries. Environ. Pollut. 310, 119831.
Wellington, J.H., 1943. The Lake Chrissie problem. S. Afr. Geogr. J. 25, 1–15.
Wenig, M., Spichtinger, N., Stohl, A., Held, G., Beirle, S., Wagner, T., Jähne, B., Platt, U., 2002. Intercontinental transport of nitrogen oxide pollution plumes. Atmos. Chem. Phys. Discuss. 2, 2151–2165.
WR2012, 2015. Water Resources of South Africa, 2012 Study – Home. https://waterresourceswr2012.co.za/ (Accessed January 29, 2023).
Yang, H., Turner, S., Rose, N.L., 2016. Mercury pollution in the lake sediments and catchment soils of anthropogenically-disturbed sites across England. Environ. Pollut. 219, 1092–1101.
Yang, H., Macario-González, L., Cohuo, S., Whitmore, T.J., Salgado, J., Peréz, L., Schwalb, A., Rose, N.L., Holmes, J., Riedinger-Whitmore, M., Hoelzmann, P., O'Dea, A., 2023. Mercury pollution history in tropical and subtropical American lakes: multiple impacts and the possible relationship with climate change. Environ. Sci. Technol. 57, 3680–3690.
Zerizghi, T., Guo, Q., Zhao, C., Okoli, C.P., 2022. Sulfur, lead, and mercury characteristics in South Africa coals and emissions from the coal-fired power plants. Environ. Earth Sci. 81, 116.
Zunckel, M., Robertson, S., Tyson, P.D., Rodhe, H., 2000. Modelled transport and deposition of sulphur over southern Africa. Atmos. Environ. 34, 2797–2808.